bioRxiv preprint doi: https://doi.org/10.1101/2020.06.04.135400; this version posted June 6, 2020. The copyright holder for this preprint (which was not certified by peer review) is the author/funder. All rights reserved. No reuse allowed without permission.

Activation of the myeloid checkpoint inhibitor LILRB3 (ILT5) elicits profound immununomodulation

Muchaala Yeboah[1], Charys Papagregoriou[1], Des C. Jones[2], H.T. Claude Chan[1], Guangan Hu[3], Justine S. McPartlan[3], Torbjörn Schiött[4], Ulrika Mattson[4], C. Ian Mockridge[1], Ulla-Carin Tornberg[4], Björn Hambe[4], Anne Ljungars[4], Mikael Mattsson[4], Ivo Tews[5,6], Stephen M. Thirdborough[1], John Trowsdale[2], Björn Frendeus[4], Jianzhu Chen[3], Mark S. Cragg[1,‡*], Ali Roghanian[1,3,‡*]

[1]Antibody & Vaccine Group, Centre for Cancer Immunology, School of Cancer Sciences, Faculty of Medicine, University of Southampton, Southampton General Hospital, Southampton, UK;

[2]Division of Immunology, Department of Pathology, University of Cambridge, Cambridge, UK;

[3]Koch Institute for Integrative Cancer Research and Department of Biology, Massachusetts Institute of Technology, Cambridge, Massachusetts, 02142, USA;

[4]BioInvent International AB, Lund, Sweden.;

[5]Institute for Life Sciences, University of Southampton, Southampton, UK;

[6]Biological Sciences, University of Southampton, Southampton, UK.

[‡] These authors contributed equally to this work and share senior authorship.

*Corresponding authors: Ali Roghanian (A.Roghanian@soton.ac.uk / aroghani@mit.edu) and Mark S Cragg (msc@soton.ac.uk)

Running title: Immunomodulating functions of LILRB3

bioRxiv preprint doi: https://doi.org/10.1101/2020.06.04.135400; this version posted June 6, 2020. The copyright holder for this preprint (which was not certified by peer review) is the author/funder. All rights reserved. No reuse allowed without permission.

Abstract

Despite advances in identifying the key immunoregulatory roles of the human leukocyte immunoglobulin (Ig)-like receptor (LILR) family members, the function of the inhibitory receptor LILRB3 (ILT5, CD85a, LIR3) remains unclear. Studies indicate a predominant myeloid expression; however, high homology within the LILR family and a relative paucity of reagents have hindered progress. To investigate its function and potential immunomodulatory capacity, a panel of LILRB3-specific monoclonal antibodies (mAb) was generated. LILBR3-specific mAb bound to discrete epitopes in either Ig-like domain two or four. LILRB3 ligation on primary human monocytes by agonistic mAb resulted in phenotypic and functional changes, leading to potent inhibition of immune responses *in vitro*, including significant reduction in T cell proliferation. Importantly, agonizing LILRB3 in humanized mice induced tolerance and permitted efficient engraftment of allogeneic cells. Our findings reveal powerful immunoregulatory functions of LILRB3 and identify it as an important myeloid immune checkpoint receptor.

bioRxiv preprint doi: https://doi.org/10.1101/2020.06.04.135400; this version posted June 6, 2020. The copyright holder for this preprint (which was not certified by peer review) is the author/funder. All rights reserved. No reuse allowed without permission.

Introduction

Molecules of the human LILR family, discovered over two decades ago (*1, 2*), are expressed on leukocytes and are commonly dysregulated in a wide range of pathologies (*3, 4*). There are six activating (LILRA1–6) and five inhibitory (LILRB1–5) LILRs that together regulate immune responses (*3*). They all display two, or four, homologous C-2 type Ig-like extracellular domains, but differ in their transmembrane and cytoplasmic regions (*2, 5*). LILRA have short truncated cytoplasmic tails with charged arginine residues in their transmembrane domains, facilitating association with the ITAM-bearing FcεR γ-chain to propagate activating signaling cascades (*6*). Conversely, LILRB have long cytoplasmic tails that contain multiple ITIM motifs, which recruit phosphatases such as SHP-1 and SHIP-1 to elicit inhibitory signaling (*2, 5*). Located at human chromosome 19q13.4, these polygenic receptors demonstrate significant allelic variation, with LILRB3 and LILRB4 (ILT3) each displaying at least 15 different variants (*2, 7-9*).

The LILRBs are proposed to act as immune checkpoints serving to control and limit overt immune responses (*3*). In agreement with this, LILRB expression is increased in suppressive (also referred to as alternatively activated or M2) macrophages and tolerogenic dendritic cells (DCs) (*10-14*). On monocytes, co-ligation of LILRB1 (ILT2) and LILRB2 (ILT4) with the activating FcγRI (CD64) results in SHP-1 activation, decreasing downstream phosphorylation events and intracellular calcium mobilization (*15*). Upon ligation with HLA class I (HLA-I) ligands, LILRB1 and LILRB2 prevent migration of DCs, and promote release of anti-inflammatory cytokines (*16*). Similarly, engagement of LILRB1 on macrophages by the common HLA-I subunit, β_2-microglobulin, on malignant cells limits their phagocytic potential (*17*). We and others have shown that activation of LILRBs renders DCs tolerogenic, inhibiting T cell responses (*10, 11, 14, 16, 18, 19*). As such, the engagement of LILRB1 and LILRB2 by HLA-G is an important immunosuppressive pathway at the fetal-maternal interface during pregnancy (*20-22*). LILRB1 is also expressed on NK cells and inhibits their cytotoxic function (*23*).

bioRxiv preprint doi: https://doi.org/10.1101/2020.06.04.135400; this version posted June 6, 2020. The copyright holder for this preprint (which was not certified by peer review) is the author/funder. All rights reserved. No reuse allowed without permission.

Although mice do not express LILRs, they possess an orthologous system comprised of two paired Ig-like receptors (PIR); the activating PIR-A and the inhibitory PIR-B. PIR-B regulates priming of cytotoxic T-lymphocytes by DCs through interaction with MHC class I expressed on $CD8^+$ cells (*24*) and negatively influences integrin signaling in neutrophils and macrophages (*25*). Furthermore, PIR-B regulates the differentiation of myeloid-derived suppressor cells (MDSCs) that aid tumor progression (*26*). Similar to PIR-B, the interaction between HLA-G and LILRB1 supports allotransplant engraftment through expansion of potent MDSC (*27, 28*).

Among the inhibitory LILRBs, LILRB3 (ILT5/LIR3/CD85a), containing 4 extracellular Ig-like domains and 4 intracellular ITIM motifs, represents an attractive immunomodulatory target because of its relative restriction to, and high expression on, myeloid cells (*3, 4*). However, due to the lack of specific reagents and model systems, its exact functions and immunoregulatory potential have not been fully explored. In this study, we addressed this by generating a bespoke panel of novel LILRB3-specific mAb, some of which were used to probe the function of LILRB3 in suitable preclinical platforms. Our data demonstrate that LILRB3 activation confers potent immunoinhibitory functions through reprograming and tolerizing of myeloid cells, and suggest that modulating its activity may provide exciting new treatment strategies in various disease settings, such as transplantation.

bioRxiv preprint doi: https://doi.org/10.1101/2020.06.04.135400; this version posted June 6, 2020. The copyright holder for this preprint (which was not certified by peer review) is the author/funder. All rights reserved. No reuse allowed without permission.

Results

Generation and characterization of a panel of fully human LILRB3-specific mAb

To study the protein expression and function of LILRB3, LILRB3-specific antibodies were identified from a human antibody phage-display library, n-CoDeR (*29, 30*). Initial alignment analysis of extracellular domains of LILRB1–5 indicated the presence of a limited number of conserved amino acid (a.a.) residues across the LILRB3 ectodomain (fig. S1A), against which specific mAb could be generated. In this regard, phages binding to the 'target', ectodomain of LILRB3 protein (present in solution, coated to a plastic surface or expressed on cells), and not to the homologous (~65% extracellular homology) 'non-target' LILRB1 ectodomain protein, were selected (Fig. 1A; fig. S1B). To increase specificity and yield, the cross-reactive phages were initially removed through a pre-selection (negative selection/depletion using 'non-target' proteins), followed by the selection itself (positive selection). Following each selection round, the selected clones were screened against the ectodomains of both LILRB1 and LILRB2 by flourometric microvolume assay technology (FMAT) and enzyme-linked immunosorbent assay (ELISA), and cross-reactive clones were further excluded from the panel. After three rounds of phage panning and enrichment, successful selection of clones specific for LILRB3 was reconfirmed by FMAT and ELISA, with target-specific phage converted to soluble scFv and screened further (Fig. 1B and C). Successful clones were selected based on binding to LILRB3 and lack of cross-reactivity to LILRB1 and LILRB2. Selected scFv clones (>200) were then sequenced and tested for binding against primary cells and LILRB transfectants using high throughput flow cytometry (Fig. 1D). Subsequently, 46 candidate target-specific clones were converted to human IgG1 (hIgG1) and, in addition to screening against LILRB1–3 transfectants, to exclude those with potential broader LILR cross-reactivity, were screened against a larger panel of LILR-expressing cell lines (Fig. 1E). Due to cross-reactivity to one or more other LILR family members, as exemplified by clone A30 (Fig. 1E, bottom panel), 30 mAb clones were further excluded at this stage. In total a panel of 16 LILRB3-specific antibodies were identified for further study. These LILRB3-specific clones were further tested and confirmed to have no cross reactivity to the mouse orthologue, PIR-B (data not shown). A selection of these mAb were then fluorochrome-labelled and used to determine the LILRB3 expression profile of human peripheral blood; demonstrating predominant staining of monocytes and to a lesser extent granulocytes (Fig. 1F and G), in agreement with previous reports (*2, 3, 5*). The

bioRxiv preprint doi: https://doi.org/10.1101/2020.06.04.135400; this version posted June 6, 2020. The copyright holder for this preprint (which was not certified by peer review) is the author/funder. All rights reserved. No reuse allowed without permission.

immunophenotyping also revealed that LILRB3 expression was significantly higher on circulatory $CD14^{+hi}/CD16^{-}$ 'classical' and $CD14^{+}/CD16^{+low}$ 'intermediate' monocytes compared with the more inflammatory $CD14^{+}/CD16^{+hi}$ 'non-classical' monocytes (Fig. 1F and G).

The selected LILRB3 mAb were then tested for their specific binding properties. Surface plasmon resonance (SPR) analysis showed that all LILRB3-specific clones bound to recombinant LILRB3-hFc protein in a dose-dependent manner (as represented by A16; Fig. 2A) and displayed a range of affinities (Table 1). Interestingly, all mAb had similar association rates ($\sim 10^{5}$), but varied in their dissociation rates by three orders of magnitude ($\sim 10^{-3}$–10^{-6}).

Cell surface epitope mapping studies were then performed and compared to a commercial mAb (clone 222821), with a series of LILRB3 extracellular domain (D) mutants displaying either all four extracellular domains (wild-type [WT]), three, two, or one domain, transiently transfected into HEK293F cells. Two distinct groups of mAb were identified: those that bound to the WT, D3 and D2 expressing cells (including clone 222821); and those that bound only the WT-transfected cells, indicating mAb binding within D2 (exemplified by A12) or D4 (exemplified by A1), respectively (Fig. 2B). Although conserved a.a. residues are present throughout the ectodomain (fig. S1A), the selected mAb were shown to bind either within D2 or D4 (6/16 and 10/16 clones, respectively; Table 1), perhaps indicating improved accessibility for these regions within the 3D structure. In agreement with this, subsequent blocking assays confirmed that a number of D2-binding mAb reduced the binding of the commercial mAb, suggesting a shared or related epitopes; whilst others did not, confirming binding to discrete epitopes (Fig. 2C and Table 1).

Subsequently, reporter cells transfected with a chimeric receptor expressing the extracellular domain of LILRB3, fused with the human CD3ζ cytoplasmic domain, were used to investigate whether the generated mAb were able to crosslink the receptor. Cross-linking results in the production of NFAT activation and the subsequent expression of GFP and is indicative of agonistic potential (*31*). Using these cells, we were able to identify two distinct groups of LILRB3 mAb, those with 'agonistic' activity capable of inducing signaling upon binding to the receptor (*e.g.*, A1) and those which were inert (*e.g.*, A28) (Fig. 2D). Collectively, these data demonstrate that highly specific, fully hIgG1 mAb were raised against LILRB3, amenable for the comprehensive evaluation of LILRB3 function.

bioRxiv preprint doi: https://doi.org/10.1101/2020.06.04.135400; this version posted June 6, 2020. The copyright holder for this preprint (which was not certified by peer review) is the author/funder. All rights reserved. No reuse allowed without permission.

LILRB3 ligation modulates T cell activation and proliferation

Accordingly, using a select number of mAb, we sought to investigate the immunomodulating effect of the LILRB3 mAb on cellular effector functions. LILRB1 has previously been shown to inhibit T cell responses; either by causing dephosphorylation of the CD3 signaling cascade, or competing with CD8 for HLA-I binding (*32, 33*). Moreover, LILRBs can indirectly inhibit T cell responses by rendering antigen-presenting cells (APC), such as monocytes and DCs tolerogenic (*13, 16, 34*). To investigate the immunomodulatory potential of LILRB3 and its ability to regulate adaptive immune responses, we utilized a T cell proliferation assay incorporating fresh PBMCs isolated from healthy human donors, as before (*35*). Fcγ receptors (FcγRs) help mediate the effects of human IgG (*36*), therefore, to study the direct F(ab):LILRB3-mediated effects of the mAb on T cell proliferation, they were first deglycosylated to reduce FcγR-IgG interactions. SDS-PAGE confirmed a decrease in molecular weight of deglycosylated mAb compared to WT controls, indicative of successful deglycosylation (Fig. 3A). The mAb were then introduced to a T cell proliferation assay where CD3 and CD28 antibodies elicit cell clustering and CFSE dilution, indicative of a significant increase in $CD8^+$ T cell proliferation, compared to non-treated controls (Fig. 3B and C). Clone A1, shown to be an agonist (Fig. 2D), significantly inhibited $CD8^+$ T cell proliferation in this assay when compared to the isotype control (Fig. 3B and C). Other LILRB3-specific mAb had either no, or subtle effects, as represented by clones A16 and A28. These data demonstrate that LILRB3 ligation by agonistic mAb suppresses T cell responses; whereas, other clones confer no inhibitory effects. Similar effects were also observed when considering $CD3^+$ $CD8^-$ T cells (predominantly $CD3^+$ $CD4^+$ T cells; Fig. 3C and not shown). When the assay was repeated with isolated T cells, no inhibition was seen, confirming that APCs within the PBMC mixture, most likely monocytes, were responsible for the effects observed (fig. S2), as expected, given the lack of expression of LILRB3 on T cells (Fig. 1F and G).

LILRB3 ligation induces immune tolerance in humanized mice

Given these data showing that T cells could be suppressed following LILRB3 ligation on myeloid cells, we next investigated the possible effects of LILRB3 modulation in an allogeneic engraftment model using humanized mice, previously reconstituted with primary human fetal hematopoietic stem/progenitor cells (HSPC) (Fig. 4A). Characterization of

bioRxiv preprint doi: https://doi.org/10.1101/2020.06.04.135400; this version posted June 6, 2020. The copyright holder for this preprint (which was not certified by peer review) is the author/funder. All rights reserved. No reuse allowed without permission.

peripheral blood leukocytes and bone marrow of adult humanized mice demonstrated that LILRB3 was expressed on and restricted to the myeloid cells, but not lymphocytes, similar to humans (Fig. 4B and fig. S3). We recently showed that allogeneic human lymphoma cells are readily rejected in humanized mice due to HLA mismatch (*37*). To test the potential of LILRB3 ligation to suppress the allogeneic immune response, adult humanized mice were treated with the agonistic LILRB3 mAb (A1) and the engraftment of allogeneic human B cell lymphoma cells, derived from an unrelated donor (*37, 38*), monitored overtime (Fig. 4A). LILRB3 mAb treatment was able to induce a state of tolerance *in vivo* and led to a successful engraftment of the donor allogeneic cells (Fig. 4C). Accordingly, LILRB3-treated tumor-bearing humanized mice subsequently succumbed to disease with high tumor burden, whereas, isotype control-treated mice readily rejected the lymphoma cells without morbidity (Fig. 4D). These observations corroborate our *in vitro* functional assays and identify LILRB3 as a key regulator of immune tolerance in an allotransplant setting. Given the expression pattern of LILRB3 on myeloid but not lymphocytic cells in both the human PBMC and humanized mice, we sought to explore the effects of the LILRB3 mAb on these cells.

LILRB3 ligation leads to transcriptional modification and M2-skewing of human APCs

To investigate the pathways and factors involved in LILRB3-mediated immunosuppression, we next investigated the transcriptomic changes in monocytes following LILRB3 engagement. Short-term (~18 hour) *in vitro* treatment of freshly-isolated human peripheral $CD14^+$ monocytes with the agonistic LILRB3 mAb (A1) caused a dramatic shift in their phenotype (Fig. 5A), with the cells displaying an elongated morphology resembling immunosuppressed M2 macrophages (*39*). In accordance with this, RNAseq analysis revealed that ligation of LILRB3 on monocytes induced a signature resembling 'M2-skewed' immunosuppressive macrophages (Fig. 5B). Concurrently, the expression of genes associated with 'M1-skewed' immunostimulatory macrophages was downregulated in LILRB3-ligated monocytes (Fig. 5B-C). These data were confirmed by qPCR for a number of the differentially regulated genes on a further 6 donors (Fig. 5D). As further evidence, we showed that the effects were dependent upon LILRB3 agonism as treatment of monocytes with a non-agonistic LILRB3 mAb (A28), despite binding the same domain, did not affect monocyte phenotype or gene expression (Fig. 5D). Gene set enrichment analysis (GSEA) of the RNAseq data showed a positive correlation with gene signatures reported for suppressive macrophages, *e.g.*, oxidative phosphorylation (*40*). Conversely, LILRB3-ligated monocyte

bioRxiv preprint doi: https://doi.org/10.1101/2020.06.04.135400; this version posted June 6, 2020. The copyright holder for this preprint (which was not certified by peer review) is the author/funder. All rights reserved. No reuse allowed without permission.

gene signatures negatively correlated with those reported for inflammatory macrophages, *e.g.*, IFN-γ and IFN-α responsive elements, as well as allograft rejection (Fig. 5E), in-line with our *in vivo* observations (Fig. 4). In summary, these data confirm that LILRB3 activation results in significant phenotypic and transcriptional alterations in human primary myeloid cells, leading to potent inhibition of downstream immune responses (Fig. 6).

bioRxiv preprint doi: https://doi.org/10.1101/2020.06.04.135400; this version posted June 6, 2020. The copyright holder for this preprint (which was not certified by peer review) is the author/funder. All rights reserved. No reuse allowed without permission.

Discussion

We previously demonstrated that ligation of LILRB1 on human monocytes induces a tolerogenic phenotype, hindering T cell responses (*16, 41*). In this study, we investigated another inhibitory LILR family member, LILRB3, whose function, largely due to lack of suitable reagents and experimental systems, is not yet fully determined. Limited previous studies investigated the consequences of LILRB3 activation on granulocytes and have demonstrated its inhibitory function on neutrophils (*42*) and basophils (*43*) in culture. Here, we largely concentrated on myelomonocytic cells and the subsequent regulation of adaptive immune responses. We, therefore, initially generated and characterized an extensive panel of fully human mAb with specificity for LILRB3 through a number of stringent panning and selection processes. Those clones showing unexpected cross-reactivity to other human LILR family members were excluded. Immunoprofiling of circulatory leukocytes from healthy donors using these highly specific mAb confirmed the reported expression of LILRB3 on myelomonocytic and granulocytic cells, but not on lymphocytes (*2, 3, 5*). This pattern of expression on myeloid and granulocytic but not lymphoid cells was confirmed in a large cohort of independent donors (>50), suggesting that, despite the polymorphic nature of LILRB3 (*2, 8, 44*), the selected antibodies recognize many, if not all, variants, which is important for the development of these reagents for therapeutic applications. Subsequent analysis showed that the LILRB3 mAb displayed a range of affinities, albeit all within the nanomolar (nM) range, with similar on-rates, but off-rates differing over three orders of magnitude. K_D values in the low nM range are generally considered to be viable drug candidates; rituximab, for example, has an 8 nM affinity for its target, CD20 (*45*). This suggests that the LILRB3 mAb generated here have potential as therapeutic agents. However, as LILRB3 shares high sequence homology (>95%) in its extracellular domain with LILRA6, there is a possibility that some LILRB3 mAb may also recognize shared epitopes on LILRA6, if co-expressed (*8*). These initial data might receive further evidence from other reagents as well as investigation as to whether LILRA6 protein is detectable in leukocyte subsets, e.g., using proteomics approaches similar to a recent study with neutrophils (*42*). Epitope mapping experiments revealed that the specific LILRB3 mAb reported here were generated against two specific ectodomains, either Ig-like domain two or four. Interestingly, none of the generated specific LILRB3 mAb bound to Ig-like domains one or three, suggesting that these domains may not contain epitopes that are unique for LILRB3, or more likely those unique residues are not exposed/accessible. Collectively, these data confirm that our LILRB3 mAb

bioRxiv preprint doi: https://doi.org/10.1101/2020.06.04.135400; this version posted June 6, 2020. The copyright holder for this preprint (which was not certified by peer review) is the author/funder. All rights reserved. No reuse allowed without permission.

will be useful tools for dissecting LILRB3's molecular mechanisms and may additionally have therapeutic benefits in relevant pathologies.

The ability of the LILRB3 mAb to influence T cell responses was variable: ranging from inhibition to indications of modest increases in proliferation, supportive of agonistic or blocking properties, respectively. Similar to LILRB1 (*16, 17, 46*), these effects are likely through manipulations of APCs, specifically monocytes, as they are the only cells expressing LILRB3 in the culture. In support of this, the agonistic LILRB3 mAb did not suppress T cell proliferation in the absence of monocytes. Binding epitopes influence the ability of mAb to modulate receptor function in many systems (*36, 47*) and so it was unsurprising to see LILRB3 mAb capable of differing functions. However, the D4-binding A1 mAb was a strong inhibitor of proliferation; whereas, other D4-binding mAb (*e.g.*, A28) had no significant effect. Therefore, domain-specific epitopes did not seem to correlate directly with LILRB3 mAb-mediated effector cell functions and may not be predictive of LILRB3 mAb function *per se*. Further detailed analyses, *e.g.*, surface alanine scanning mutagenesis (*47*) and/or structural studies, are required to define the specific extracellular epitopes engaged by the selected LILRB3 mAb and to investigate their influence on receptor activity.

Our observations demonstrating immunoinhibitory activities downstream of LILRB3 were further confirmed in the reconstituted humanized mouse model. In this system, where LILRB3 is present only on the hematopoietic cells, and predominantly monocytes, in the absence of appreciable numbers of neutrophils, ligation of LILRB3 with an agonistic LILRB3 mAb prior to injection of allogeneic lymphoma cells (*37, 38*) induced tolerance *in vivo* and enabled subsequent tumor engraftment. This demonstrates the capacity of LILRB3 to exert profound immunosuppressive effects that may be exploited in therapeutic settings, such as autoimmunity and transplantation, where transient induction of immune tolerance will be beneficial.

Although typically regarded as an orphan receptor, our earlier studies suggest that LILRB3 may associate with cytokeratin-associated proteins such as those exposed on necrotic cancer cells (*31*). Others have also identified angiopoietin-like protein 5 and bacteria, such as

bioRxiv preprint doi: https://doi.org/10.1101/2020.06.04.135400; this version posted June 6, 2020. The copyright holder for this preprint (which was not certified by peer review) is the author/funder. All rights reserved. No reuse allowed without permission.

Staphylococcus aureus, as a source of potential ligands (*48, 49*). Therefore, our data provide a strong mechanism of action whereby such endogenous or pathogenic ligands may be able to subvert immune responses by ligating LILRB3 during an ongoing immune response.

To investigate the pathways and factors involved in LILRB3-mediated immunosuppression, we investigated the transcriptomic changes in isolated peripheral myeloid cells following LILRB3 activation. Over one hundred genes were differentially regulated in primary human monocytes following LILRB3 ligation, some of which are known to be modulated in M2 macrophages and TAMs (*12, 50*). Amphiregulin (AREG) was among the genes whose expression was significantly upregulated in LILRB3-ligated monocytes. AREG is an epidermal growth factor-like growth factor, responsible for inducing tolerance and immunosuppression, via various mechanisms including enhancement of Treg activity (*51*). Furthermore, AREG is overexpressed in tumor-associated DCs (*52*) and suppressive/M2 macrophages (*53*) and has been suggested to play a crucial role in immunosuppression and cancer progression (*54*). Such LILRB3-inducible factors may be responsible for the suppression observed in our T cell assays. Our ongoing efforts aim to interrogate these findings further and define the mechanisms responsible for LILRB3-mediated suppression of immune responses at molecular and cellular levels, *e.g.*, via siRNA knockdown of AREG in monocytes and validation of differentially regulated genes in the humanized mouse models. A recent study investigating the mode of action of Glatiramer acetate (Copaxone), a peptide-based drug licensed in the late 1990's, used to treat patients with the relapsing-remitting form of multiple sclerosis that ameliorates autoimmunity, identified LILRB2 and LILRB3 as potential ligands (*55*). On the other hand, blocking human LILRB2 with antagonistic mAb on human myeloid cells is able to promote their pro-inflammatory activity and enhance antitumor responses in preclinical models (*17*); and a LILRB2 mAb (MK-4830) recently entered phase I clinical trials (NCT03564691) for advanced solid tumors. Furthermore, recent data by Zhang and colleagues suggest that LILRB4 signaling in leukemia cells mediates T cell suppression and supports tumor cell dissemination to distal organs (*56*). These recent compelling reports further support our findings, demonstrating that activation of human LILRB3 induces immunosuppression via reprogramming of myeloid cells (*i.e.*, reducing M1-like maturation and promoting suppressive function).

bioRxiv preprint doi: https://doi.org/10.1101/2020.06.04.135400; this version posted June 6, 2020. The copyright holder for this preprint (which was not certified by peer review) is the author/funder. All rights reserved. No reuse allowed without permission.

In conclusion, our findings show that LILRB3 activation on primary human myeloid cells exerts potent immunoinhibitory functions and that LILRB3-specific mAb are potentially powerful immunomodulatory agents, with broad application ranging from transplantation to autoimmunity and beyond, where fine-tuning of immune responses through myeloid cell activity is desired.

bioRxiv preprint doi: https://doi.org/10.1101/2020.06.04.135400; this version posted June 6, 2020. The copyright holder for this preprint (which was not certified by peer review) is the author/funder. All rights reserved. No reuse allowed without permission.

Materials and Methods

Ethics Statement

All research with human samples and mice was performed in compliance with institutional guidelines, the Declaration of Helsinki and the US Department of Health and Human Services Guide for the Care and Use of Laboratory Animals. The Committee on Animal Care at Massachusetts Institute of Technology (MIT) reviewed and approved the studies described here. Animal experiments performed at the University of Southampton were approved by the local ethical committees and were performed under Home Office license P4D9C89EA.

All human samples (adult peripheral blood and fetal liver) were collected anonymously with informed consent by a third party and purchased for research. For human peripheral blood, ethical approval for the use of clinical samples was obtained by the Southampton University Hospitals NHS Trust; from the Southampton and South West Hampshire Research Ethics Committee following provision of informed consent. Primary chronic lymphocytic leukemia (CLL) samples were released from the Human Tissue Authority licensed University of Southampton, Cancer Science Unit Tissue Bank as part of the LPD study REC number 228/02/T.

Cell culture

Cell lines were grown at 37°C in either RPMI 1640 medium supplemented with 10% heat-inactivated fetal calf serum (FCS) (Sigma-Aldrich, UK), 100 U/ml Penicillin-Streptomycin, 2 mM Glutamine and 1 mM Pyruvate (Thermo Fisher Scientific, UK) in a humidified incubator with 5% CO_2, Freestyle 293F media, in 8% CO_2, shaking at 130 rpm, or Freestyle CHO media (Thermo Fisher Scientific, UK) with 8 mM Glutamine, in 8% CO_2, shaking at 140 rpm.

Antibody generation and production

Generation of LILRB3 antibodies

Generation of LILRB3-specific mAb was performed using the nCoDeR phage-display library (*29*). Three consecutive panning rounds were performed, as well as a pre-panning step. In the panning, human (h) Fc fusion proteins containing the extracellular domains of LILRB1 and

bioRxiv preprint doi: https://doi.org/10.1101/2020.06.04.135400; this version posted June 6, 2020. The copyright holder for this preprint (which was not certified by peer review) is the author/funder. All rights reserved. No reuse allowed without permission.

LILRB3 (LILRB-hFc) were used as 'non-target' or 'target', respectively. These proteins were produced in transiently transfected HEK293 cells followed by purification on protein A, as described previously (*36*). CHO-S cells transiently transfected to express the various LILRB proteins were also used as targets/non-targets in the panning.

In panning 1, BioInvent n-CoDeR® scFv were selected using biotinylated in-house produced recombinant LILRB3-hFc recombinant fusion proteins (captured with streptavidin-coated Dynabeads®) with or without competition or LILRB1-hFc coated to etched polystyrene balls (Polysciences, US) or plastic immunotubes. Binding phages were eluted by trypsin digestion and amplified on plates using standard procedures (*57*). The amplified phages from panning 1 were used for panning 2, the process repeated, and the amplified phages from panning 2 used in panning 3. In the third panning round, however, amplified phages from all 3 strategies were combined and selected against LILRB–expressing CHO-S cells, prior to making the final LILRB3-specific mAb selection.

Next, the LILRB3-positive scFv from the enriched phage repertoires from panning 3 were re-cloned to allow soluble scFv expression in *E. coli*. The soluble scFv fragments expressed by individual clones were tested for binding against LILRB-transfected CHO-S cells using FMAT, and recombinant LILRB protein by ELISA. This allowed the identification of clones binding specifically to LILRB3. Clones were then further reduced in a tertiary screen against CHO-S cells expressing LILRB1-3 and primary cells (PBMCs) using a high throughput flow cytometry screening system and data analyzed by TIBCO Spotfire® software (TIBCO, USA). Clones showing specific patterns of binding to LILRB3 were sequenced, yielding LILRB3-specific mAb.

Production of full-length IgG

The unique scFv identified above were cloned into a eukaryotic expression system allowing transient expression of full-length IgG in HEK293-EBNA cells. The antibodies were then purified from the culture supernatants using Protein A affinity chromatography as previously described (*36*).

Production of deglycosylated IgG

To allow dissection of Fc- and Fab-dependent effector functions, IgG were deglycosylated using PNGase F (Promega) with 0.05 U of PNGase/µg of IgG, at 37°C for at least 15 hours. Deglycosylation was confirmed by reduction in size of the heavy chain on SDS-PAGE.

bioRxiv preprint doi: https://doi.org/10.1101/2020.06.04.135400; this version posted June 6, 2020. The copyright holder for this preprint (which was not certified by peer review) is the author/funder. All rights reserved. No reuse allowed without permission.

Production of domain mutant constructs

Using wild-type LILRB3 cDNA isolated from a healthy donor PBMCs, a series of domain mutant DNA constructs were generated by overlap PCR to express 1, 2 or 3 LILRB3 Ig-like domains (with domains identified based on annotations in Uniprot) for comparison to WT LILRB3 (4 domains). The gene constructs were then cloned into pcDNA3.

Cell Transfections

10 x 10^6 HEK293F cells were transiently transfected with 10 µg of plasmid DNA by lipofection using 233 fectin with Optimem 1 Media (Thermo Fisher Scientific, UK).

Preparation of human leukocytes

PBMC were isolated from leukocyte blood cones (Blood Transfusion Services, Southampton General Hospital) by gradient density centrifugation using lymphoprep (Axis-Shield, UK) and used for subsequent experiments, as before (*58*).

Flow cytometry

For cell surface staining of PBMCs or whole blood, cells were blocked with 2% human AB serum (Sigma-Aldrich, UK) for 10 minutes on ice and then stained with the relevant APC-labelled mAb or hIgG1 isotype (BioInvent, Sweden), alongside the following cell surface markers: CD14-PE (eBioscience, UK), CD20-A488 (Rituximab, in house), CD3-PE-Cy7, CD56-APC-Cy7 or CD15-Pacific Blue, CD15-PE and CD66B-FITC (all Biolegend, UK). Cells were stained for 30 minutes at 4°C and then washed twice, first in 10% red blood cell (RBC) lysis buffer (Serotec, UK) for PBMCs or 1x Erythrolyse RBC Lysing Buffer (Biorad, UK) for whole blood, and then with FACS wash (PBS, 1% BSA, 10 mM NaN_3), before acquisition on a FACSCalibur or FACSCanto II (BD Biosciences, USA) and analyzed with FlowJo software (BD Biosciences, USA).

bioRxiv preprint doi: https://doi.org/10.1101/2020.06.04.135400; this version posted June 6, 2020. The copyright holder for this preprint (which was not certified by peer review) is the author/funder. All rights reserved. No reuse allowed without permission.

For assays to determine if mAb bound to similar cross-blocking epitopes 1 x 10^6 PBMCs were blocked with 2% human AB serum for 10 minutes and stained with 10 µg/ml unconjugated LILRB3 mAb for 30 minutes at 4°C. The cells were then stained with directly-conjugated LILRB3 mAb (clone 222821; mouse IgG2a; R&D Systems, UK) for 20 minutes at 4°C, before washing and acquisition using a FACSCalibur.

For LILRB3 epitope mapping studies, LILRB3-domain mutant-transfected HEK293F cells were stained with the relevant LILRB3 mAb for 25 minutes at 4°C, washed twice, stained with an anti-human-PE secondary (Jackson ImmunoResearch, USA) for 20 minutes at 4°C, before washing and acquisition using a FACSCalibur.

For staining of 2B4 reporter cells expressing LILR-A1, -A2, -A5, -B1, -B2, -B3, -B4, or -B5 (or non-transfected controls) (*31, 59*) cells were stained with 10 µg/ml LILRB mAb and incubated at 37°C with 5% CO_2, overnight. The following day, the cells were washed and stained with a secondary anti-hIgG antibody (Jackson ImmunoResearch, USA) at 4°C, for 45 minutes. The cells were washed and acquisition performed using a FACScan (BD Biosciences, USA) and data analyzed with FlowJo software (BD Biosciences, USA).

Surface plasmon resonance (SPR)

SPR was performed with the Biacore T100 (GE Healthcare, UK) as per the manufacturer's instructions. LILRB3-hFc recombinant protein (extracellular LILRB3 domain with a hFc tag) was used as the ligand and immobilized by amine coupling onto a series S sensor chip (CM5). Various LILRB3 mAb were used as 'analytes' and flowed across the chip, and SPR measured. K_D values were calculated from the 'Univalent' model of 1:1 binding by Kd [1/s] / Ka [1/Ms], using the Biacore™ T100 Evaluation Software (GE Healthcare, UK).

T cell Proliferation assay

PBMCs (1-2 x 10^7) were labelled with 2 µM carboxyfluorescein succinimidyl ester (CSFE) at room temperature for 10 minutes. An equal volume of FCS was then added to quench labeling for 1 minute, prior to washing. Cells were subsequently resuspended in serum-free CTL medium (Immunospot, Germany) and plated at 1x10^5 cells/well in a 96-well round-bottom plate (Corning, UK). Cells were then stimulated with 0.02 µg/ml CD3 (clone OKT3,

bioRxiv preprint doi: https://doi.org/10.1101/2020.06.04.135400; this version posted June 6, 2020. The copyright holder for this preprint (which was not certified by peer review) is the author/funder. All rights reserved. No reuse allowed without permission.

in-house), 5 µg/ml CD28 (clone CD28.2; Biolegend, UK) and 10 µg/ml LILRB3 antibodies or a relevant isotype. Plates were then incubated at 37°C for 4 days, after which time cells were stained with 5 µg/ml CD8-APC (clone SK1; Biolegend, UK), harvested and CSFE dilution measured by flow cytometry, as a readout for T cell proliferation.

Hematopoietic stem/progenitor cell (HSPC) isolation and generation of humanized mice

Humanized mice were generated, as described (*37*). In brief, human fetal livers were obtained from aborted fetuses at 15–23 weeks of gestation, in accordance with the institutional ethical guidelines (Advanced Bioscience Resources, Inc., USA). All women gave written informed consent for the donation of their fetal tissue for research. Fresh tissue was initially cut into small pieces and digested with collagenase VI (2 mg/ml; Roche) for 30 minutes at 37°C. Single-cell suspensions were prepared by passing the digested tissue through a 100 µm cell strainer (BD Biosciences, USA). HSPCs were purified using a $CD34^+$ selection kit (Stem Cell Technologies, Canada); the purity of $CD34^+$ cells was 90%–99%. Viability was determined through trypan blue exclusion of dead cells. All cells were isolated under sterile conditions and injected into NSG mice.

NSG mice were purchased from the Jackson Laboratories (Bar Harbor, USA) and maintained under specific pathogen-free conditions in the animal facilities at MIT. To reconstitute mice, newborn pups (less than 2 days old) were irradiated with 100 cGy using a Gamma radiation source and injected intracardially with $CD34^+$ cells (~2×10^5 cells/recipient), as reported previously (*37*). Around 12 weeks later, human leukocyte cell reconstitution of PBMCs was determined by flow cytometry and calculated as follows: % human $CD45^+$ cell / (% human $CD45^+$ cell + % mouse $CD45^+$ cell). Mice with ≥ 40% human $CD45^+$ leukocytes were used in subsequent experiments.

***In vivo* allograft assay**

Fully reconstituted humanized mice were injected with 200 µg LILRB3 mAb (clone A1) or an isotype-matched (hIgG1) control on day 0 and day 4, i.v. and i.p, respectively. On day 7, cohorts of mice were injected i.p. with 1 x 10^7 luciferase-positive human 'double-hit' B cell lymphoma cells (*37, 38*), derived from unrelated donors. Lymphoma cell growth was

bioRxiv preprint doi: https://doi.org/10.1101/2020.06.04.135400; this version posted June 6, 2020. The copyright holder for this preprint (which was not certified by peer review) is the author/funder. All rights reserved. No reuse allowed without permission.

monitored over time using an IVIS Spectrum-bioluminescent imaging system, as before (*37*). Mice with palpable tumors were sacrificed and Kaplan-Meier survival curves plotted.

Transcriptome analysis

To assess LILRB3-mediated transcriptional changes on monocytes, human peripheral blood monocytes were isolated from freshly prepared PBMCs taken from healthy donors using an EasySep™ Human Monocyte Enrichment Kit (negative selection cell; StemCell Technologies, Canada). Cells were incubated in CTL medium supplemented with 100 U/ml Penicillin-Streptomycin, 2 mM Glutamine and HEPES buffer and treated with 10 µg/ml of an isotype control or an agonistic LILRB3 mAb (clone A1; hIgG1). 18 hours later, cells were lysed in RLT lysis buffer containing β-mercaptoethanol and total RNA extracted using the RNeasy micro kit (Qiagen, USA). Total RNA was assessed for quality and quantified using a total RNA 6000 Nano LabChip on a 2100 Bioanalyzer (Agilent Inc., USA) and cDNA libraries prepared and sequenced according to the Illumina TruSeq RNA Sample Preparation Guide for SMARTer Universal Low Input RNA Kit (Clontech, USA) and a HiSeq 2000 system (Illumina, USA). RNAseq outputs were aligned to hg19 using Bowtie2 v2.2.3 (*60*). The number of mapped reads were quantified by RSEM v1.2.15 (*61*). Differential expression analysis between paired samples before and after treatment was performed using edgeR (*62*) with p <0.05 and >2 fold-change cut-offs. Differentially expressed genes were annotated using online functional enrichment analysis tool DAVID (http://david.ncifcrf.gov/) (*63*). Gene-set enrichment analysis (GSEA) was performed using Broad Institute Software (*64*), with the gene list pre-ranked according to logFC values from the edgeR output. For comparison of gene-set expression, M1 and M2 macrophage gene sets (*50*) were obtained from the Molecular Signature Database (http://software.broadinstitute.org/gsea/msigdb/). Heatmaps were visualized with MeV (*65*). Raw sequences are deposited in the database of Gene Expression Omnibus with accession ID GSE151675.

Quantitative PCR (qPCR)

Probe-based qPCR was used to amplify cDNA in 20µl reactions performed in triplicate for each sample condition in a PCR plate (Bio-Rad, UK), as per the manufacturer's protocol. The 96-well plate was run on a C1000 Thermal Cycler CFX96 Real-time System PCR machine

bioRxiv preprint doi: https://doi.org/10.1101/2020.06.04.135400; this version posted June 6, 2020. The copyright holder for this preprint (which was not certified by peer review) is the author/funder. All rights reserved. No reuse allowed without permission.

(Bio-Rad, Kidlington, UK). The CFX manager software (Bio-Rad, Kidlington, UK), was used for data acquisition and analysis of gene expression initially recorded as cycle threshold values (Ct). The Ct values were normalised to housekeeping gene Glyceraldehyde 3-phosphate dehydrogenase (GAPDH) and standardised to gene expression levels in isotype control-treated samples.

Statistics

Paired two-tailed T-tests were performed for both the immunophenotyping and T cell proliferation data; straight bars indicate median values. On bar graphs, where at least 3 experiments were performed, error bars represent standard deviation. Kaplan-Meier plots were analyzed by Log-rank test. One-way ANOVA with Bonferroni's multiple comparisons test were performed for qPCR data analysis. Statistical analysis was performed using GraphPadPrism (v6-8).

bioRxiv preprint doi: https://doi.org/10.1101/2020.06.04.135400; this version posted June 6, 2020. The copyright holder for this preprint (which was not certified by peer review) is the author/funder. All rights reserved. No reuse allowed without permission.

References

1. L. Borges, M. L. Hsu, N. Fanger, M. Kubin, D. Cosman, A family of human lymphoid and myeloid Ig-like receptors, some of which bind to MHC class I molecules. *J Immunol* **159**, 5192-5196 (1997).
2. M. Colonna *et al.*, A common inhibitory receptor for major histocompatibility complex class I molecules on human lymphoid and myelomonocytic cells. *The Journal of experimental medicine* **186**, 1809-1818 (1997).
3. W. van der Touw, H. M. Chen, P. Y. Pan, S. H. Chen, LILRB receptor-mediated regulation of myeloid cell maturation and function. *Cancer Immunol Immunother* **66**, 1079-1087 (2017).
4. L. E. Hudson, R. L. Allen, Leukocyte Ig-Like Receptors - A Model for MHC Class I Disease Associations. *Front Immunol* **7**, 281 (2016).
5. L. Borges, M. L. Hsu, N. Fanger, M. Kubin, D. Cosman, A family of human lymphoid and myeloid Ig-like receptors, some of which bind to MHC class I molecules. *J Immunol* **159**, 5192-5196 (1997).
6. H. Nakajima, J. Samaridis, L. Angman, M. Colonna, Human myeloid cells express an activating ILT receptor (ILT1) that associates with Fc receptor gamma-chain. *J Immunol* **162**, 5-8 (1999).
7. C. C. Chang *et al.*, Polymorphism and linkage disequilibrium of immunoglobulin-like transcript 3 gene. *Hum Immunol* **69**, 284-290 (2008).
8. M. R. Lopez-Alvarez, D. C. Jones, W. Jiang, J. A. Traherne, J. Trowsdale, Copy number and nucleotide variation of the LILR family of myelomonocytic cell activating and inhibitory receptors. *Immunogenetics* **66**, 73-83 (2014).
9. K. Hirayasu, H. Arase, Functional and genetic diversity of leukocyte immunoglobulin-like receptor and implication for disease associations. *J Hum Genet* **60**, 703-708 (2015).
10. F. W. Velten, K. Duperrier, J. Bohlender, P. Metharom, S. Goerdt, A gene signature of inhibitory MHC receptors identifies a BDCA3(+) subset of IL-10-induced dendritic cells with reduced allostimulatory capacity in vitro. *Eur J Immunol* **34**, 2800-2811 (2004).
11. C. C. Chang *et al.*, Tolerization of dendritic cells by T(S) cells: the crucial role of inhibitory receptors ILT3 and ILT4. *Nat Immunol* **3**, 237-243 (2002).
12. M. Beyer *et al.*, High-resolution transcriptome of human macrophages. *PLoS One* **7**, e45466 (2012).
13. J. S. Manavalan *et al.*, High expression of ILT3 and ILT4 is a general feature of tolerogenic dendritic cells. *Transpl Immunol* **11**, 245-258 (2003).
14. J. Banchereau *et al.*, Immunoglobulin-like transcript receptors on human dermal CD14+ dendritic cells act as a CD8-antagonist to control cytotoxic T cell priming. *Proc Natl Acad Sci U S A* **109**, 18885-18890 (2012).
15. N. A. Fanger *et al.*, The MHC class I binding proteins LIR-1 and LIR-2 inhibit Fc receptor-mediated signaling in monocytes. *Eur J Immunol* **28**, 3423-3434 (1998).
16. N. T. Young *et al.*, The inhibitory receptor LILRB1 modulates the differentiation and regulatory potential of human dendritic cells. *Blood* **111**, 3090-3096 (2008).
17. A. A. Barkal *et al.*, Engagement of MHC class I by the inhibitory receptor LILRB1 suppresses macrophages and is a target of cancer immunotherapy. *Nat Immunol* **19**, 76-84 (2018).
18. M. K. Rochat *et al.*, Maternal vitamin D intake during pregnancy increases gene expression of ILT3 and ILT4 in cord blood. *Clin Exp Allergy* **40**, 786-794 (2010).
19. M. Brenk *et al.*, Tryptophan deprivation induces inhibitory receptors ILT3 and ILT4 on dendritic cells favoring the induction of human CD4+CD25+ Foxp3+ T regulatory cells. *J Immunol* **183**, 145-154 (2009).
20. M. G. Petroff, P. Sedlmayr, D. Azzola, J. S. Hunt, Decidual macrophages are potentially susceptible to inhibition by class Ia and class Ib HLA molecules. *J Reprod Immunol* **56**, 3-17 (2002).

bioRxiv preprint doi: https://doi.org/10.1101/2020.06.04.135400; this version posted June 6, 2020. The copyright holder for this preprint (which was not certified by peer review) is the author/funder. All rights reserved. No reuse allowed without permission.

21. R. Apps, L. Gardner, A. M. Sharkey, N. Holmes, A. Moffett, A homodimeric complex of HLA-G on normal trophoblast cells modulates antigen-presenting cells via LILRB1. *Eur J Immunol* **37**, 1924-1937 (2007).
22. L. Lombardelli *et al.*, HLA-G5 induces IL-4 secretion critical for successful pregnancy through differential expression of ILT2 receptor on decidual CD4(+) T cells and macrophages. *J Immunol* **191**, 3651-3662 (2013).
23. B. Favier, J. Lemaoult, E. Lesport, E. D. Carosella, ILT2/HLA-G interaction impairs NK-cell functions through the inhibition of the late but not the early events of the NK-cell activating synapse. *FASEB J* **24**, 689-699 (2010).
24. S. Endo, Y. Sakamoto, E. Kobayashi, A. Nakamura, T. Takai, Regulation of cytotoxic T lymphocyte triggering by PIR-B on dendritic cells. *Proc Natl Acad Sci U S A* **105**, 14515-14520 (2008).
25. S. Pereira, H. Zhang, T. Takai, C. A. Lowell, The inhibitory receptor PIR-B negatively regulates neutrophil and macrophage integrin signaling. *J Immunol* **173**, 5757-5765 (2004).
26. N. S. Wilson *et al.*, An Fcgamma receptor-dependent mechanism drives antibody-mediated target-receptor signaling in cancer cells. *Cancer cell* **19**, 101-113 (2011).
27. W. Zhang, S. Liang, J. Wu, A. Horuzsko, Human Inhibitory Receptor ILT2 Amplifies CD11b(+)Gr1(+) Myeloid-Derived Suppressor Cells that Promote Long-Term Survival of Allografts. *Transplantation* **86**, 1125-1134 (2008).
28. J. Wu *et al.*, Isoforms of human leukocyte antigen-G and their inhibitory receptors in human kidney allograft acceptance†. *Human Immunology* **70**, 988-994 (2009).
29. E. Soderlind *et al.*, Recombining germline-derived CDR sequences for creating diverse single-framework antibody libraries. *Nature biotechnology* **18**, 852-856 (2000).
30. A. Roghanian *et al.*, Antagonistic human FcgammaRIIB (CD32B) antibodies have anti-tumor activity and overcome resistance to antibody therapy in vivo. *Cancer cell* **27**, 473-488 (2015).
31. D. C. Jones *et al.*, Allele-specific recognition by LILRB3 and LILRA6 of a cytokeratin 8-associated ligand on necrotic glandular epithelial cells. *Oncotarget* **7**, 15618-15631 (2016).
32. D. Saverino *et al.*, The CD85/LIR-1/ILT2 inhibitory receptor is expressed by all human T lymphocytes and down-regulates their functions. *J Immunol* **165**, 3742-3755 (2000).
33. M. Shiroishi *et al.*, Human inhibitory receptors Ig-like transcript 2 (ILT2) and ILT4 compete with CD8 for MHC class I binding and bind preferentially to HLA-G. *Proc Natl Acad Sci U S A* **100**, 8856-8861 (2003).
34. C. C. Chang *et al.*, BCL6 Is Required for Differentiation of Ig-Like Transcript 3-Fc-Induced CD8(+) T Suppressor Cells. *J Immunol* **185**, 5714-5722 (2010).
35. K. Hussain *et al.*, Upregulation of FcgammaRIIb on monocytes is necessary to promote the superagonist activity of TGN1412. *Blood* **125**, 102-110 (2015).
36. L. N. Dahal, A. Roghanian, S. A. Beers, M. S. Cragg, FcgammaR requirements leading to successful immunotherapy. *Immunological reviews* **268**, 104-122 (2015).
37. A. Roghanian *et al.*, Cyclophosphamide Enhances Cancer Antibody Immunotherapy in the Resistant Bone Marrow Niche by Modulating Macrophage FcgammaR Expression. *Cancer Immunol Res* **7**, 1876-1890 (2019).
38. I. Leskov *et al.*, Rapid generation of human B-cell lymphomas via combined expression of Myc and Bcl2 and their use as a preclinical model for biological therapies. *Oncogene* **32**, 1066-1072 (2013).
39. F. Y. McWhorter, T. Wang, P. Nguyen, T. Chung, W. F. Liu, Modulation of macrophage phenotype by cell shape. *Proc Natl Acad Sci U S A* **110**, 17253-17258 (2013).
40. S. Galvan-Pena, L. A. O'Neill, Metabolic reprograming in macrophage polarization. *Front Immunol* **5**, 420 (2014).
41. R. C. Khanolkar *et al.*, Leukocyte Ig-Like receptor B1 restrains dendritic cell function through increased expression of the NF-kappaB regulator ABIN1/TNIP1. *J Leukoc Biol*, (2016).

bioRxiv preprint doi: https://doi.org/10.1101/2020.06.04.135400; this version posted June 6, 2020. The copyright holder for this preprint (which was not certified by peer review) is the author/funder. All rights reserved. No reuse allowed without permission.

42. Y. Zhao *et al.*, The Orphan Immune Receptor LILRB3 Modulates Fc Receptor-Mediated Functions of Neutrophils. *J Immunol* **204**, 954-966 (2020).
43. D. E. Sloane *et al.*, Leukocyte immunoglobulin-like receptors: novel innate receptors for human basophil activation and inhibition. *Blood* **104**, 2832-2839 (2004).
44. A. A. Bashirova *et al.*, Diversity of the human LILRB3/A6 locus encoding a myeloid inhibitory and activating receptor pair. *Immunogenetics* **66**, 1-8 (2014).
45. M. D. Pescovitz, Rituximab, an anti-cd20 monoclonal antibody: history and mechanism of action. *Am J Transplant* **6**, 859-866 (2006).
46. C. S. Wagner *et al.*, Human cytomegalovirus-derived protein UL18 alters the phenotype and function of monocyte-derived dendritic cells. *J Leukoc Biol* **83**, 56-63 (2008).
47. X. Yu *et al.*, Complex Interplay between Epitope Specificity and Isotype Dictates the Biological Activity of Anti-human CD40 Antibodies. *Cancer cell* **33**, 664-675 e664 (2018).
48. M. Nakayama *et al.*, Paired Ig-like receptors bind to bacteria and shape TLR-mediated cytokine production. *J Immunol* **178**, 4250-4259 (2007).
49. J. Zheng *et al.*, Inhibitory receptors bind ANGPTLs and support blood stem cells and leukaemia development. *Nature* **485**, 656-660 (2012).
50. F. O. Martinez, S. Gordon, M. Locati, A. Mantovani, Transcriptional profiling of the human monocyte-to-macrophage differentiation and polarization: new molecules and patterns of gene expression. *J Immunol* **177**, 7303-7311 (2006).
51. D. M. W. Zaiss, W. C. Gause, L. C. Osborne, D. Artis, Emerging functions of amphiregulin in orchestrating immunity, inflammation, and tissue repair. *Immunity* **42**, 216-226 (2015).
52. Y. L. Hsu *et al.*, Lung tumor-associated dendritic cell-derived amphiregulin increased cancer progression. *J Immunol* **187**, 1733-1744 (2011).
53. P. Vlaicu *et al.*, Monocytes/macrophages support mammary tumor invasivity by co-secreting lineage-specific EGFR ligands and a STAT3 activator. *BMC Cancer* **13**, 197 (2013).
54. B. Busser, L. Sancey, E. Brambilla, J. L. Coll, A. Hurbin, The multiple roles of amphiregulin in human cancer. *Biochim Biophys Acta* **1816**, 119-131 (2011).
55. W. van der Touw *et al.*, Glatiramer Acetate Enhances Myeloid-Derived Suppressor Cell Function via Recognition of Paired Ig-like Receptor B. *J Immunol* **201**, 1727-1734 (2018).
56. M. Deng *et al.*, LILRB4 signalling in leukaemia cells mediates T cell suppression and tumour infiltration. *Nature* **562**, 605-609 (2018).
57. N. Olsson *et al.*, Proteomic Analysis and Discovery Using Affinity Proteomics and Mass Spectrometry. *Mol Cell Proteomics* **10**, (2011).
58. A. Roghanian *et al.*, Filament-associated TSGA10 protein is expressed in professional antigen presenting cells and interacts with vimentin. *Cell Immunol* **265**, 120-126 (2010).
59. L. E. Hogan, D. C. Jones, R. L. Allen, Expression of the innate immune receptor LILRB5 on monocytes is associated with mycobacteria exposure. *Sci Rep* **6**, 21780 (2016).
60. B. Langmead, C. Trapnell, M. Pop, S. L. Salzberg, Ultrafast and memory-efficient alignment of short DNA sequences to the human genome. *Genome Biol* **10**, R25 (2009).
61. B. Li, C. N. Dewey, RSEM: accurate transcript quantification from RNA-Seq data with or without a reference genome. *BMC Bioinformatics* **12**, 323 (2011).
62. M. D. Robinson, D. J. McCarthy, G. K. Smyth, edgeR: a Bioconductor package for differential expression analysis of digital gene expression data. *Bioinformatics* **26**, 139-140 (2010).
63. D. W. Huang *et al.*, DAVID Bioinformatics Resources: expanded annotation database and novel algorithms to better extract biology from large gene lists. *Nucleic Acids Res* **35**, W169-175 (2007).
64. A. Subramanian *et al.*, Gene set enrichment analysis: a knowledge-based approach for interpreting genome-wide expression profiles. *Proc Natl Acad Sci U S A* **102**, 15545-15550 (2005).
65. A. I. Saeed *et al.*, TM4: a free, open-source system for microarray data management and analysis. *Biotechniques* **34**, 374-378 (2003).

bioRxiv preprint doi: https://doi.org/10.1101/2020.06.04.135400; this version posted June 6, 2020. The copyright holder for this preprint (which was not certified by peer review) is the author/funder. All rights reserved. No reuse allowed without permission.

Authorship

Contribution: AR and MSC were grant holders, initiated the research proposals, supervised the project and wrote the manuscript. MY, TS, UM, UT, BH, AL and MM generated human LILRB3 mAb and performed the initial screening. MY characterized the mAb and performed the *in vitro* functional assays. HTCC supported the molecular biology and CP and JSM supported the *in vitro* assays. JT provided reagents and edited the manuscript. BF provided expert advice on the mAb generation and edited the manuscript. JC provided expert advice on the *in vivo* assays and edited the manuscript. AR performed the *in vivo* experiments in humanized mice. DCJ, designed DNA constructs used to generate antibodies and performed specificity assays against LILR transfectants. CIM performed SPR assays. GH and SMT analyzed the RNAseq data. IT provided expert advice on the epitope mapping and edited the manuscript.

Conflict-of-interest disclosure

MSC is a retained consultant for BioInvent International and has performed educational and advisory roles for Baxalta, Boehringer Ingleheim, Merck GdA and Roche. He has received research funding from Bioinvent International, Roche, Gilead, Iteos, UCB and GSK. AR receives funding from BioInvent International. TS, UM, UT, BH, AL, MM and BF are employees of BioInvent International.

Acknowledgments and Grant Support

We would like to thank the Antibody and Vaccine Group antibody production team, Profs Tim Elliott (University of Southampton) and Jean-Michel Sallenave (Université Paris Diderot) for review of the manuscript; Drs Francesco Forconi and Ian Tracey (University of Southampton) for provision of CLL samples. We would like to thank the Koch Institute Flow Cytometry (Glenn Paradis), Bioinformatics and Computing (Stuart Levin) and Animal Imaging and Preclinical Testing cores (Scott Malstrom) for their technical assistance.

bioRxiv preprint doi: https://doi.org/10.1101/2020.06.04.135400; this version posted June 6, 2020. The copyright holder for this preprint (which was not certified by peer review) is the author/funder. All rights reserved. No reuse allowed without permission.

This work was supported by an iCASE studentship awarded to AR, BF and MSC to support MY from the BBSRC and BioInvent International AB, Sweden. AR was a recipient of a Blood Cancer UK Visiting Fellowship (14043). Work in the JT lab was supported by European Research Council (ERC) under the European Union's Horizon 2020 research and innovation programme (grant agreement No: 695551).

bioRxiv preprint doi: https://doi.org/10.1101/2020.06.04.135400; this version posted June 6, 2020. The copyright holder for this preprint (which was not certified by peer review) is the author/funder. All rights reserved. No reuse allowed without permission.

Figure legends

Fig. 1. Generation of fully human mAb against LILRB3. (**A**) Schematic of antibody generation by phage display via three independent 'panning' techniques; *(i)* immobilized target (LILRB3), *(ii)* biotinylated target and excess non-target (LILRB1), and *(iii)* LILRB3-transfectant cell lines (from left to right). Biopanning was performed against generated target protein using a scFv library; 'non-target' cross-reactive scFv clones were eluted off at each panning stage and target-specific scFv clones were then converted to a soluble format, sequenced and screened by various cell- and protein-based assays. (**B-C**) Screening of generated LILRB3 clones. (**B**) FMAT and (**C**) ELISA were performed and scFv clones screened against LILRB3 target and LILRB1/LILRB2 non-target transfected CHO-S cells and extracellular LILRB1 protein, respectively. MFI of binding to each target was calculated, with target-specific scFv depicted in yellow, non-target scFv in blue and the irrelevant isotype control shown in green. (**D**) Screening of LILRB3 scFv clones by high throughput flow cytometry. PBMCs or LILR-transfected CHO-S cells were incubated with His-tagged scFv supernatants, followed by secondary anti-His staining. Where transfected CHO-S cells were used, LILRB1- and LILRB2-transfected cells were used as non-targets for LILRB3. Clones were compared against both gated $CD14^+$ monocytes and target transfected CHO-S cells, with LILRB3 specific clones highlighted in yellow, non-specific clones in red and the isotype control in green. (**E**) Specificity of LILRB3 clones against human LILR-transfected 2B4 cells. LILRB3 mAb were tested against cells stably transfected with the indicated LILR family members by flow cytometry; a representative specific clone (A16; top panel) and a non-specific cross-reactive clone (A30; bottom panel) shown. (**F-G**) Testing the specificity of directly fluorochrome-labeled LILRB3 clones against primary cells by flow cytometry. (**F**) Fresh whole peripheral blood stained with either APC-labelled LILRB3 (represented by clone A16) or an irrelevant human (h) IgG1 isotype control as well as various leukocyte surface markers, as indicated. Dot plots and histograms are representative of multiple donors indicating gating of each leukocyte subset as indicated: T cells, B cells and NK cells, monocytes and granulocytes. (**G**) Graph showing relative expression of LILRB3 on each leukocyte subset. Two-tailed paired T-test performed (* $p < 0.05$**;** ** $p < 0.005$); $n = 5$ independent donors (each color represents an individual donor).

bioRxiv preprint doi: https://doi.org/10.1101/2020.06.04.135400; this version posted June 6, 2020. The copyright holder for this preprint (which was not certified by peer review) is the author/funder. All rights reserved. No reuse allowed without permission.

Fig. 2. Characterization of LILRB3 antibodies. (**A**) LILRB3 mAb affinity assessed by SPR. LILRB3-hFc recombinant protein was immobilized and various LILRB3 mAb flowed across the chip. Representative LILRB3 clone A16 shown. (**B**) LILRB3 domain epitope mapping. HEK293F cell transfected with either WT LILRB3 (full-length extracellular portion), D1-3, D1-2 or D1 were stained with LILRB3 clones, followed by an anti-hIgG secondary antibody. Schematic of domain constructs and restriction digest of each construct shown (top panel). Histograms showing staining of two representative clones differentially binding to color-coded WT (D4), D1-3, D1-2 and D1-expressing cells (bottom panel; n = 3 independent experiments). (**C**) Ability of generated mAb to cross-block binding of commercial LILRB3 mAb (clone 222821). PBMCs were stained with unconjugated LILRB3 antibody clones and subsequently stained with a directly-conjugated 222821 mAb and analyzed by flow cytometry; representative clones displayed (A1 non-blocking; A12 partial blocking), as indicated. (**D**) LILRB3 2B4 reporter cells were incubated with 10 µg/ml LILRB3 antibodies overnight to assess receptor signaling potential as judged by GFP induction measured by flow cytometry; representative clones with percentage of GFP expression shown.

Fig. 3. LILRB3 ligation regulates T cell activation and proliferation. CFSE-labelled PBMCs were stimulated with antibodies against human CD3 (0.02 µg/ml) and CD28 (5 µg/ml) in the presence or absence of isotype control (iso ctrl) or LILRB3 mAb (10 µg/ml) and proliferation measured through CFSE dilution after 3-5 days. (**A**) LILRB3 mAb were deglycosylated (Degly) through PNGase-treatment, as confirmed by SDS-PAGE; representative clone A1 shown. (**B**) Assessing T cell activation and proliferation following treatment. Light microscopy images following PBMC stimulation in culture. $CD8^+$ T cell proliferation was assessed through CFSE dilution; representative plots, histograms (% proliferation indicated) and microscopy images shown (10x magnification). (**C**) Assessing the effects of deglycosylated LILRB3 mAb on T cell proliferation. CFSE dilution of $CD8^+$ T cells, treated with the representative LILRB3 mAb was assessed by flow cytometry. Data normalized to anti-CD3/CD28-treated samples and mean represented by solid bars. Two-tailed paired T-test performed (*** $p < 0.0001$); n = 13-20 independent donors (each color represents an individual donor).

bioRxiv preprint doi: https://doi.org/10.1101/2020.06.04.135400; this version posted June 6, 2020. The copyright holder for this preprint (which was not certified by peer review) is the author/funder. All rights reserved. No reuse allowed without permission.

Fig. 4. LILRB3 ligation induces tolerance *in vivo*. (**A**) Schematic of the generation of humanized mice and subsequent treatment regimens and monitoring. (**B**) Expression of LILRB3 on human myeloid cells in humanized mice. Representative flow cytometry plots (gated on live single cells) showing gating strategy and the restricted expression of LILRB3 on $hCD45^+$ peripheral blood $hCD14^+$ myeloid cells; isotype control in pink, LILRB3 in blue. (**C**) The effect of agonistic LILRB3 mAb on engraftment of allogeneic cells in humanized mice. Age- and sex-matched humanized mice were injected with 200 µg LILRB3 mAb (clone A1) or an isotype-matched (hIgG1) control mAb (iso ctrl) on day 0 and 4, i.v. and i.p, respectively. On day 7, mice were injected i.p. with $1x10^7$ non-autologous $luciferase^+$ human lymphoma cells. Lymphoma cell growth was monitored over time using an IVIS imager; and (**D**) humanized mice were sacrificed upon the development of signs of terminal tumor development. Survival data was analyzed using log-rank test ($p < 0.01$); representative data from 3 independent experiments (3 individual HSPC donors) shown ($n = 3$ mice/group).

Fig. 5. Human LILRB3 ligation reprograms human primary myeloid cells. Freshly isolated human peripheral $CD14^+$ monocytes were treated with an isotype control (iso ctrl) or a human LILRB3 mAb (clone A1) and then assessed. (**A**) Agonistic LILRB3 mAb affects monocyte morphology. Light microscopy images following overnight treatment of freshly-isolated $CD14^+$ monocytes with indicated mAb in culture (10x magnification). (**B**) Transcriptomic analysis of LILRB3-treated monocytes reveals upregulation of M2-associated genes compered to controls. RNA was extracted from cells following mAb treatment (~18 hours) and subjected to RNA sequencing. Red depicts genes that were significantly upregulated and green depicts genes that were significantly downregulated compared to isotype control treated-cells ($n = 4$ independent donors). (**C**) Ligation of LILRB3 on primary human $CD14^+$ monocytes induces M2-polarized genes. GSEA graph showing a significant enrichment for M2-polarizing genes in LILRB3-treated monocytes versus isotype control, respectively. UP; upregulated, NES; normalized enrichment score = -1.68; FWER; familywise-error rate p <0.001. (**D**) qPCR analysis of selected genes following LILRB3 ligation on monocytes using an agonistic LILRB3 mAb (A1), a non-agonistic LILRB3 mAb (A28) or an isotype control (iso). Data were normalized to GAPDH mRNA levels and standardized to the levels of isotype control-treated monocytes. Fold difference data were log_{10} transformed. One-way ANOVA with Bonferroni's multiple comparisons test was performed, $n = 5$-6 independent donors (* $p < 0.005$). (**E**) GSEA analysis showing negative

bioRxiv preprint doi: https://doi.org/10.1101/2020.06.04.135400; this version posted June 6, 2020. The copyright holder for this preprint (which was not certified by peer review) is the author/funder. All rights reserved. No reuse allowed without permission.

correlation with 'IFN-γ' (NES=-2.17; FWER $p < 0.001$), 'IFN-α' (NES=-2.3; FWER $p < 0.001$) and 'allograft rejection' (NES=-1.58; FWER p = 0.14) signaling elements and positive correlation with 'oxidative phosphorylation' (NES=2; FWER $p < 0.001$).

Fig. 6. Mechanism of action of LILRB3 activation on myeloid cells. Schematic diagram demonstrating the proposed immunosuppressive function of LILRB3 following ligation on APCs.

bioRxiv preprint doi: https://doi.org/10.1101/2020.06.04.135400; this version posted June 6, 2020. The copyright holder for this preprint (which was not certified by peer review) is the author/funder. All rights reserved. No reuse allowed without permission.

Table 1. Summary of binding domain, blocking potential and affinity measurements ('Univalent' model of 1:1 binding assessed by SPR) for the selected LILRB3-specific mAb (hIgG1).

Clone ID	Ig-like domain	K_D (M)	Block Ab?
1 (A1)	4	3.12×10^{-10}	N
2 (A12)	2	5.30×10^{-10}	Y
3	4	2.92×10^{-10}	N
4 (A16)	4	2.88×10^{-9}	N
5	2	1.04×10^{-9}	Y
6	2	1.55×10^{-9}	N
7	4	3.85×10^{-10}	N
8 (A28)	4	1.46×10^{-9}	N
9	4	9.84×10^{-9}	N
10	2	3.71×10^{-10}	N
11	4	1.37×10^{-9}	N
12	4	1.24×10^{-10}	N
13	4	3.25×10^{-9}	N
14	2	3.05×10^{-10}	N
15	4	1.56×10^{-9}	N
16	2	1.68×10^{-8}	N
222821	2	1.47×10^{-11}	-

222821 represents the commercial LILRB3 mAb (mIgG2a)

Yes (Y) and No (N) for blocking clone 222821 indicated.

bioRxiv preprint doi: https://doi.org/10.1101/2020.06.04.135400; this version posted June 6, 2020. The copyright holder for this preprint (which was not certified by peer review) is the author/funder. All rights reserved. No reuse allowed without permission.

Supplementary figure legends

Fig. S1. Topological structure of LILRB3 ectodomain and schematic of LILRB3-specific mAb selection strategy. (**A**) Topological representation of the predicted extracellular domains of human LILRB3 (accession no. O75022) and its conserved a.a. residues, as aligned against LILRB1 (accession no. Q8NHL6), LILRB2 (accession no. Q8N423), LILRB4 (accession no. Q8NHJ6) and LILRB5 (accession no. O75023). Each predicted Ig-like domain (D1-4) has been separately color-coded and the conserved a.a. residues identified by red rhombus symbols. Source: UniProt and Protter. (**B**) Three 'selection' rounds were performed to generate LILRB3-specific mAbs by phage display. Three different methods to display the target protein were utilized: biotinylated target captured on streptavidin magnetic beads with competition *(A)*, biotinylated target without competition *(B)*, and immobilized protein coated on plastic polystyrene beads in the first two selection rounds, followed by cells expressing the target in selection around three using all phages from all three techniques used in panning two *(C)*. Throughout the panning rounds, LILRB1 was used as a non-target and as a competitor for LILRB3. 50 nM biotinylated non-target was used in the pre-selection for strategies where biotinylated protein was used *(A, B)*. 10 µg/ml non-target was used for strategies where coated protein was used *(C)*. No pre-selection was required for the cell strategies *(3C)*. Red border indicates completion with excess non-target protein was used.

Fig. S2. T cell proliferation is not affected by agonistic LILRB3 mAb in the absence of myeloid cells. Fresh PBMCs or purified T cells, isolated from matched PBMCs using a human CD3 negative selection kit, were CFSE-labeled and then cultured in the presence of soluble 0.02 µg/ml or 5 µg/ml plate-bound OKT3 mAb and either 10 µg/ml of isotype control (pink) or an agonistic LILRB3 mAb (blue). Proliferation was measured through CFSE dilution on day 4 by flow cytometry. Representative histogram of 3 independent experiments shown for each culture.

bioRxiv preprint doi: https://doi.org/10.1101/2020.06.04.135400; this version posted June 6, 2020. The copyright holder for this preprint (which was not certified by peer review) is the author/funder. All rights reserved. No reuse allowed without permission.

Fig. S3. Expression of LILRB3 on bone marrow-resident myeloid cells in humanized mice. Expression of LILRB3 on freshly isolated hCD45$^+$ bone marrow myeloid cells in humanized mice. Representative (3 mice/group, from 3 independent HSPC donors) flow cytometry plots (gated on live single cells) showing gating strategy and the restricted expression of LILRB3 on hCD14$^+$ myeloid cells ~3 months post engraftment of HSPCs; isotype control in pink, LILRB3 in blue.

Fig. 1.

bioRxiv preprint doi: https://doi.org/10.1101/2020.06.04.135400; this version posted June 6, 2020. The copyright holder for this preprint (which was not certified by peer review) is the author/funder. All rights reserved. No reuse allowed without permission.

A

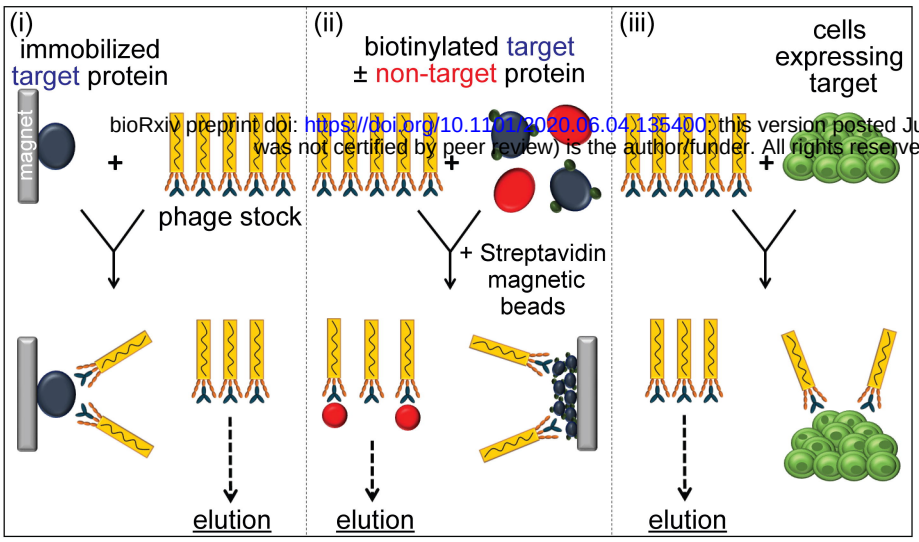

B

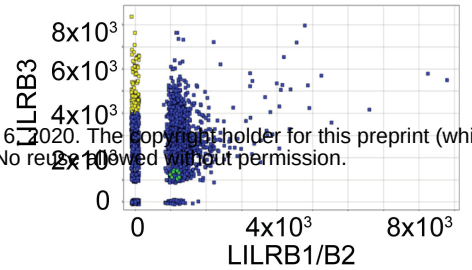

C

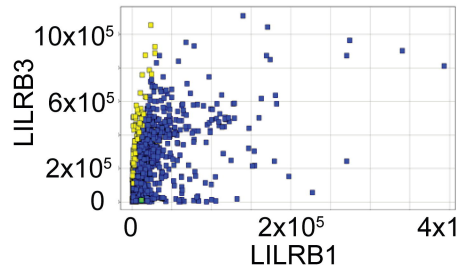

D

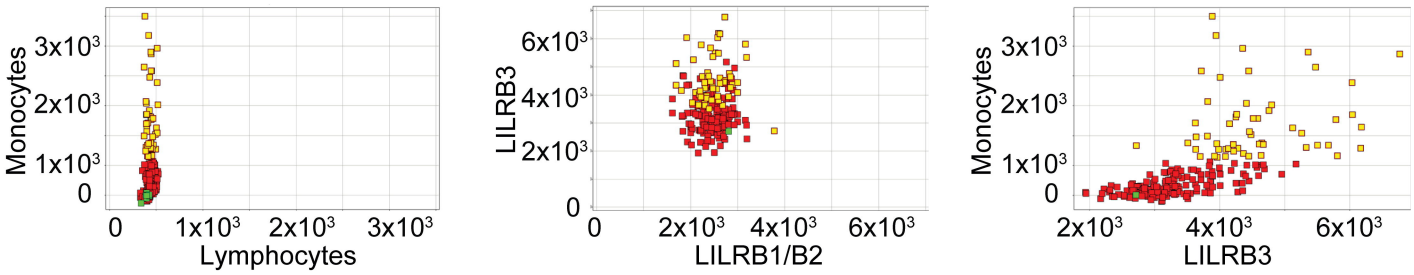

E

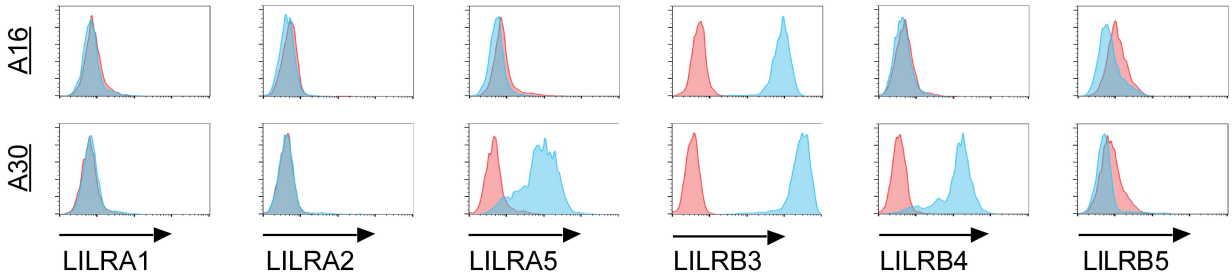

F

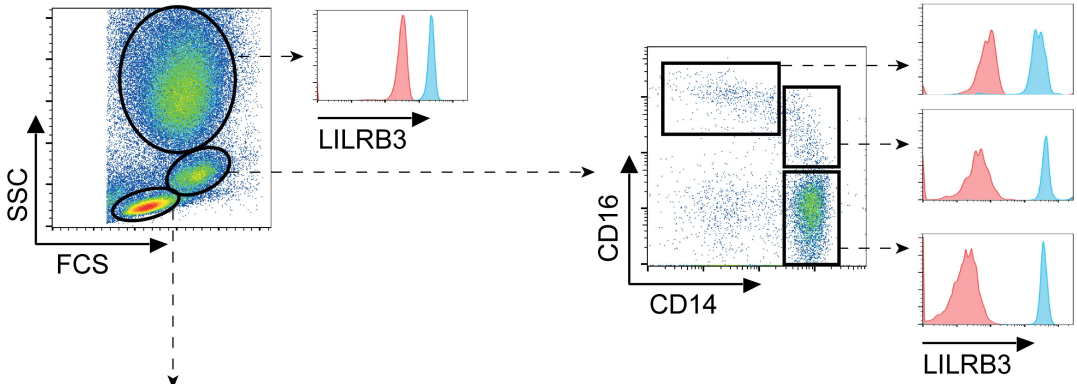

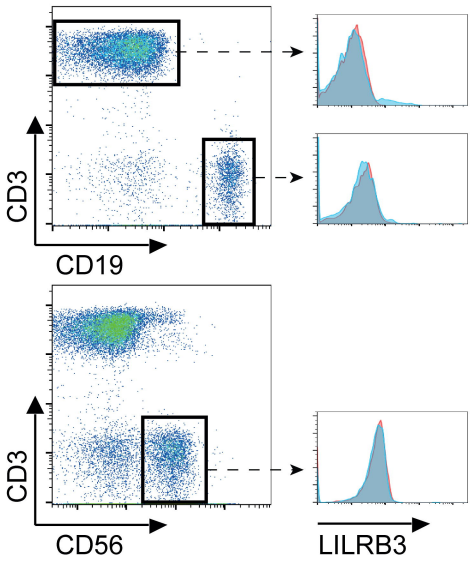

G

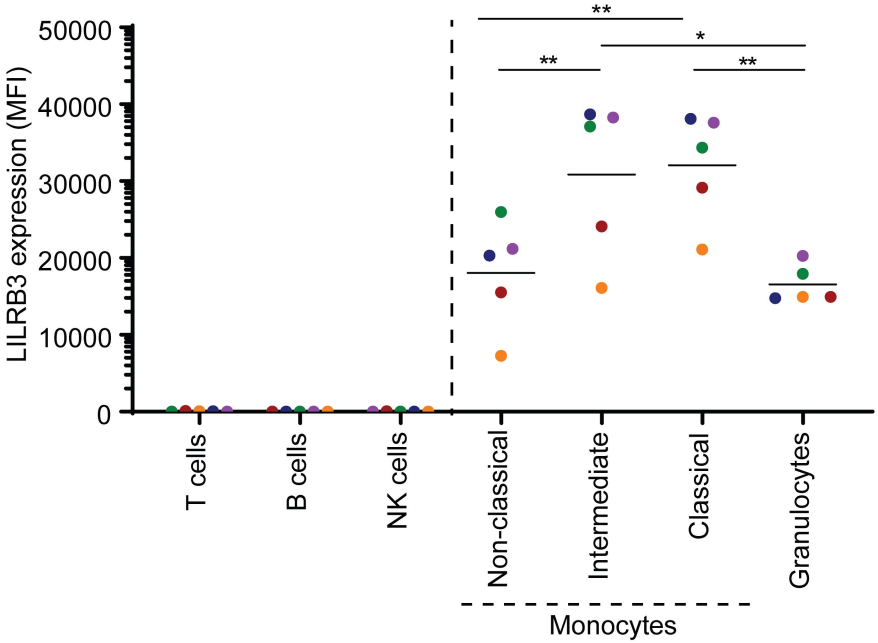

Fig. 2.

A

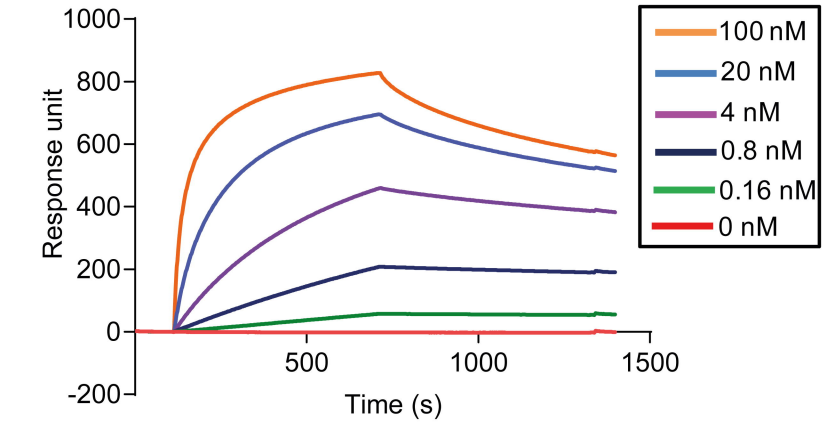
Response unit
1000
800
600
400
200
0
-200
500
1000
1500
Time (s)
100 nM
20 nM
4 nM
0.8 nM
0.16 nM
0 nM

B

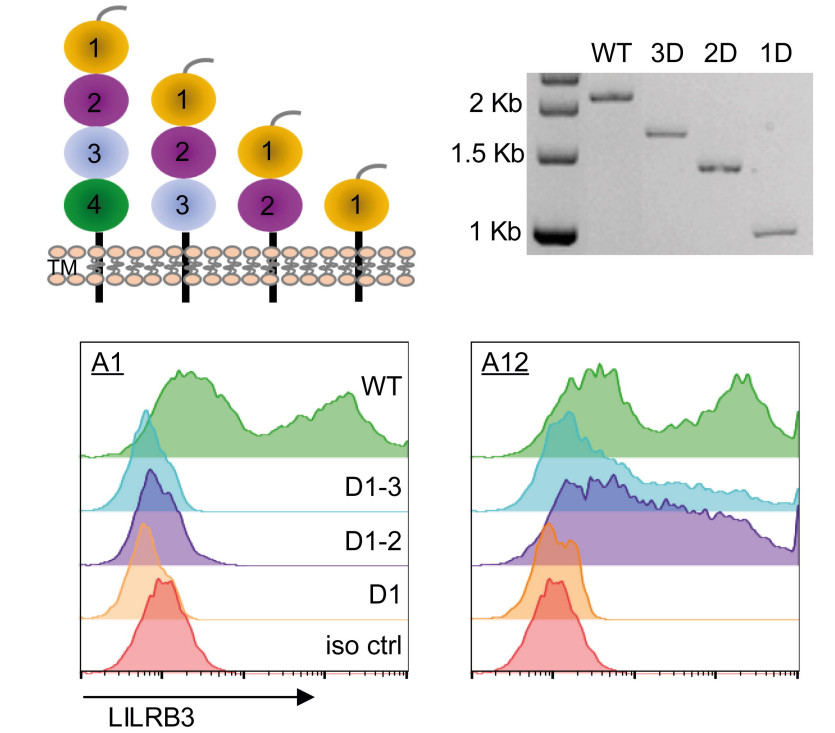
1
2
3
4
TM
WT
3D
2D
1D
2 Kb
1.5 Kb
1 Kb
A1
WT
D1-3
D1-2
D1
iso ctrl
A12
LILRB3

C

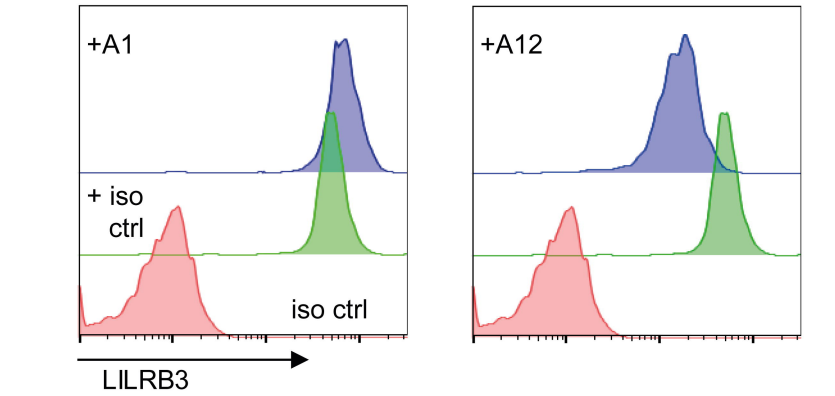
+A1
+ iso ctrl
iso ctrl
+A12
LILRB3

D

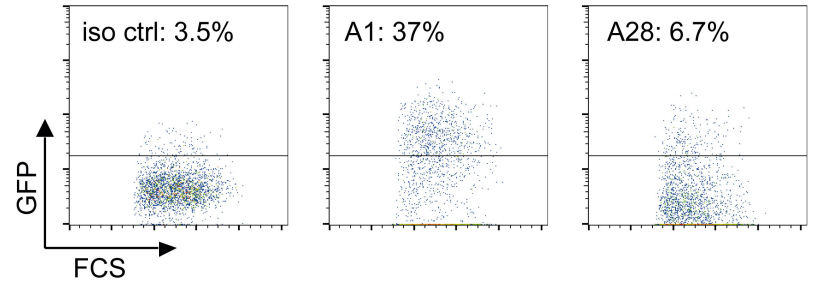
iso ctrl: 3.5%
A1: 37%
A28: 6.7%
GFP
FCS

Fig. 3.

A

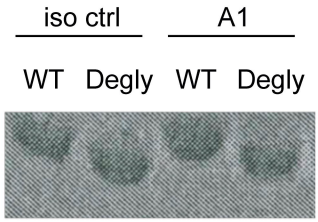
iso ctrl
A1
WT
Degly
WT
Degly

B

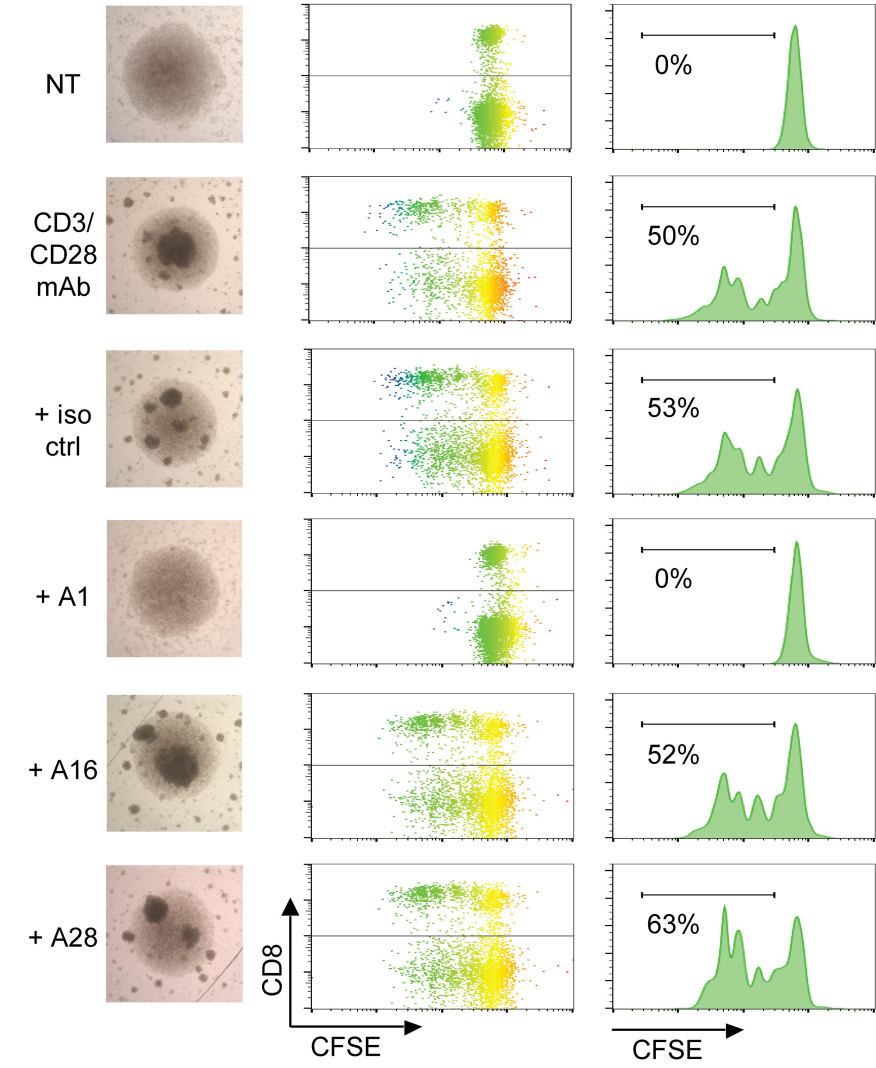
NT
CD3/
CD28
mAb
+ iso
ctrl
+ A1
+ A16
+ A28
0%
50%
53%
0%
52%
63%
CD8
CFSE
CFSE

C

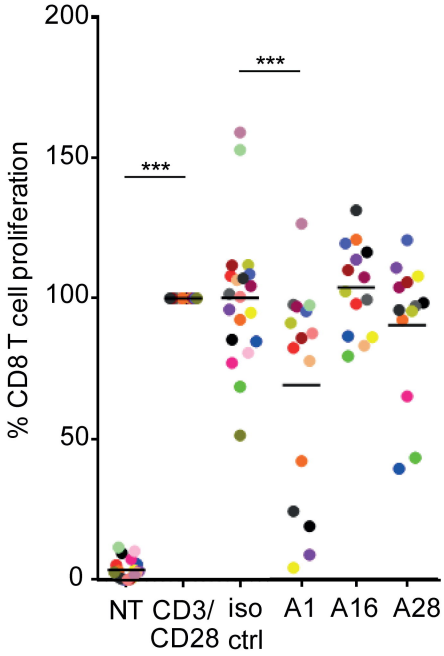
% CD8 T cell proliferation
200
150
100
50
0
***
***
NT
CD3/
CD28
iso
ctrl
A1
A16
A28

Fig. 4.

A

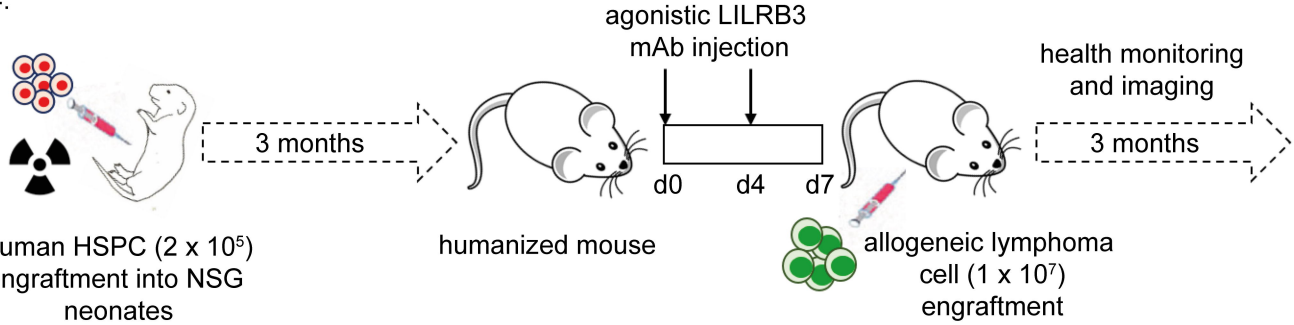
agonistic LILRB3
mAb injection
health monitoring
and imaging
3 months
3 months
d0
d4
d7
human HSPC (2 x 10⁵)
engraftment into NSG
neonates
humanized mouse
allogeneic lymphoma
cell (1 x 10⁷)
engraftment

B

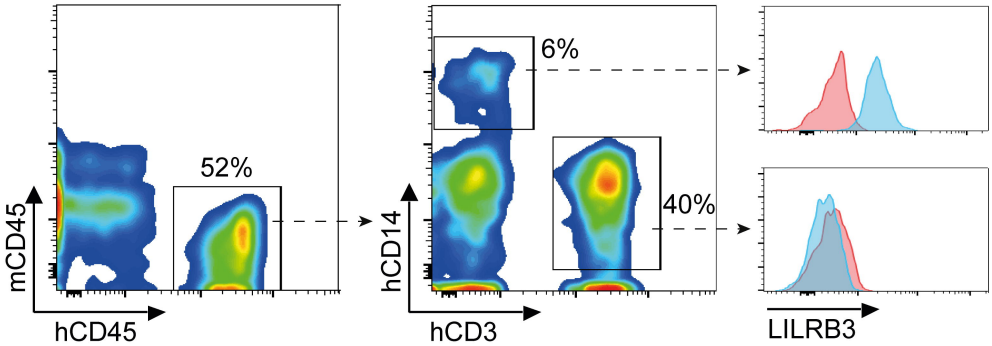
52%
mCD45
hCD45
6%
40%
hCD14
hCD3
LILRB3

C

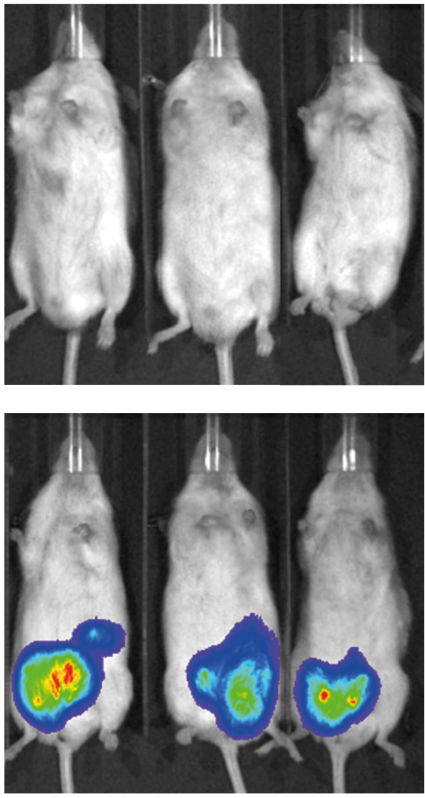
+ iso ctrl
+ LILRB3 mAb

D

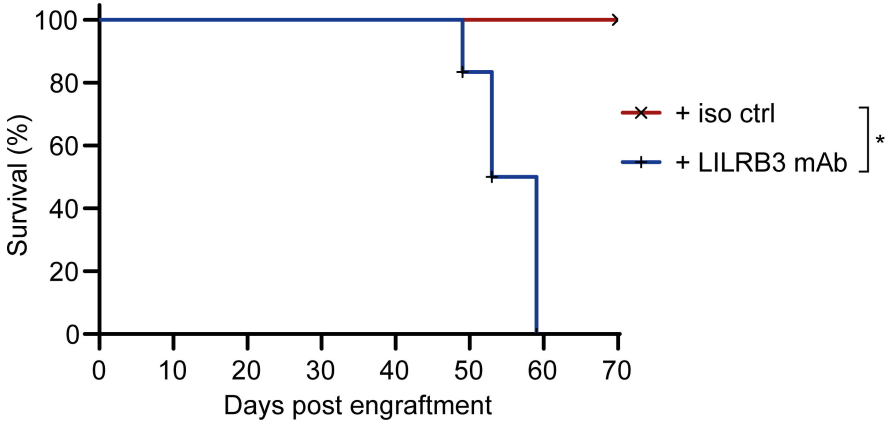
Survival (%)
100
80
60
40
20
0
0
10
20
30
40
50
60
70
Days post engraftment
+ iso ctrl
+ LILRB3 mAb
*

Fig. 5.

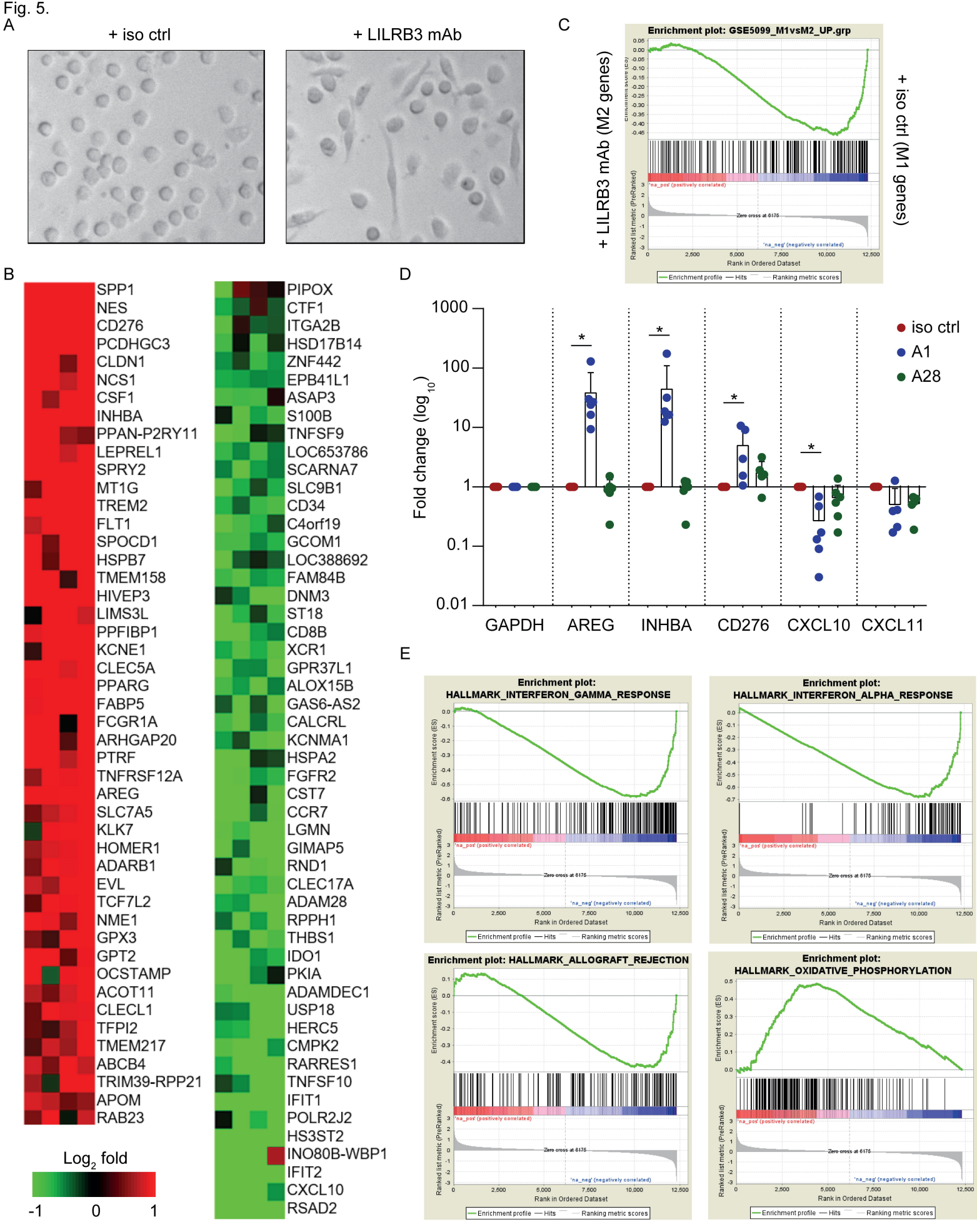
A
+ iso ctrl
+ LILRB3 mAb
C
Enrichment plot: GSE5099_M1vsM2_UP.grp
+ LILRB3 mAb (M2 genes)
+ iso ctrl (M1 genes)
Rank in Ordered Dataset
Enrichment profile
Hits
Ranking metric scores
B
SPP1
NES
CD276
PCDHGC3
CLDN1
NCS1
CSF1
INHBA
PPAN-P2RY11
LEPREL1
SPRY2
MT1G
TREM2
FLT1
SPOCD1
HSPB7
TMEM158
HIVEP3
LIMS3L
PPFIBP1
KCNE1
CLEC5A
PPARG
FABP5
FCGR1A
ARHGAP20
PTRF
TNFRSF12A
AREG
SLC7A5
KLK7
HOMER1
ADARB1
EVL
TCF7L2
NME1
GPX3
GPT2
OCSTAMP
ACOT11
CLECL1
TFPI2
TMEM217
ABCB4
TRIM39-RPP21
APOM
RAB23
PIPOX
CTF1
ITGA2B
HSD17B14
ZNF442
EPB41L1
ASAP3
S100B
TNFSF9
LOC653786
SCARNA7
SLC9B1
CD34
C4orf19
GCOM1
LOC388692
FAM84B
DNM3
ST18
CD8B
XCR1
GPR37L1
ALOX15B
GAS6-AS2
CALCRL
KCNMA1
HSPA2
FGFR2
CST7
CCR7
LGMN
GIMAP5
RND1
CLEC17A
ADAM28
RPPH1
THBS1
IDO1
PKIA
ADAMDEC1
USP18
HERC5
CMPK2
RARRES1
TNFSF10
IFIT1
POLR2J2
HS3ST2
INO80B-WBP1
IFIT2
CXCL10
RSAD2
Log2 fold
-1
0
1
D
Fold change (log10)
1000
100
10
1
0.1
0.01
iso ctrl
A1
A28
GAPDH
AREG
INHBA
CD276
CXCL10
CXCL11
E
Enrichment plot: HALLMARK_INTERFERON_GAMMA_RESPONSE
Enrichment plot: HALLMARK_INTERFERON_ALPHA_RESPONSE
Enrichment plot: HALLMARK_ALLOGRAFT_REJECTION
Enrichment plot: HALLMARK_OXIDATIVE_PHOSPHORYLATION

Fig. 6.

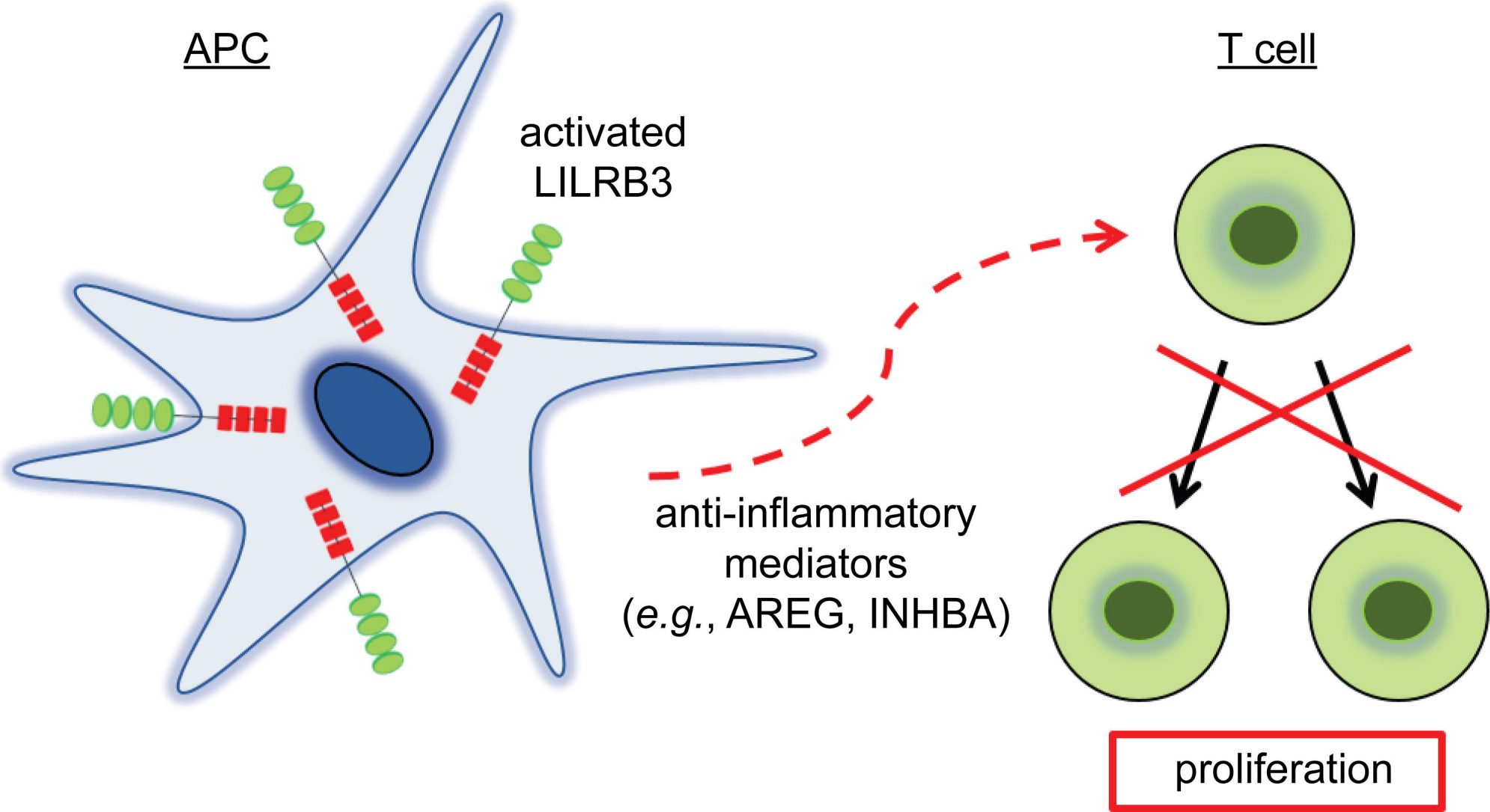
APC
T cell
activated
LILRB3
anti-inflammatory
mediators
(e.g., AREG, INHBA)
proliferation

Fig. S1.

A

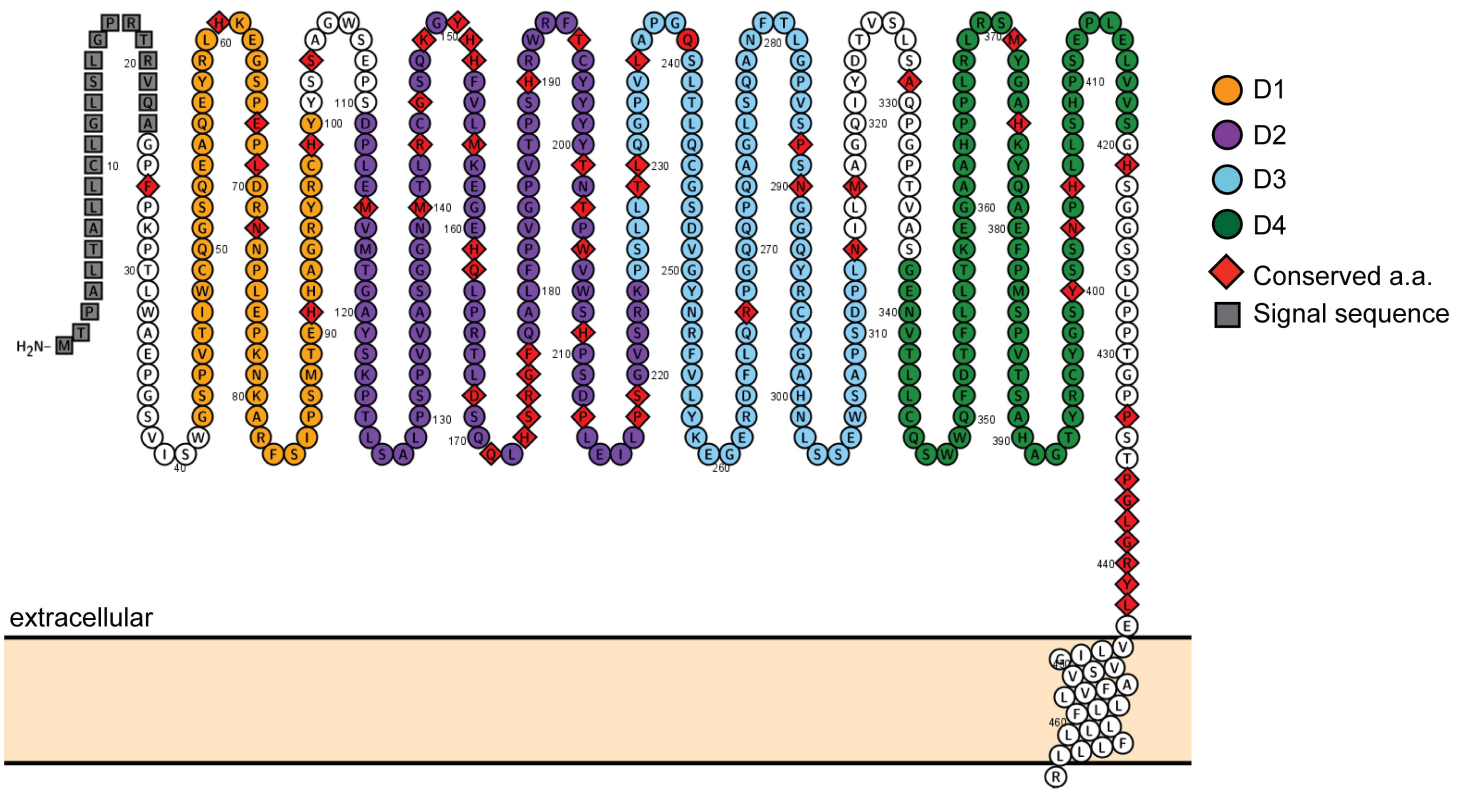
D1
D2
D3
D4
Conserved a.a.
Signal sequence
H2N-
extracellular

B

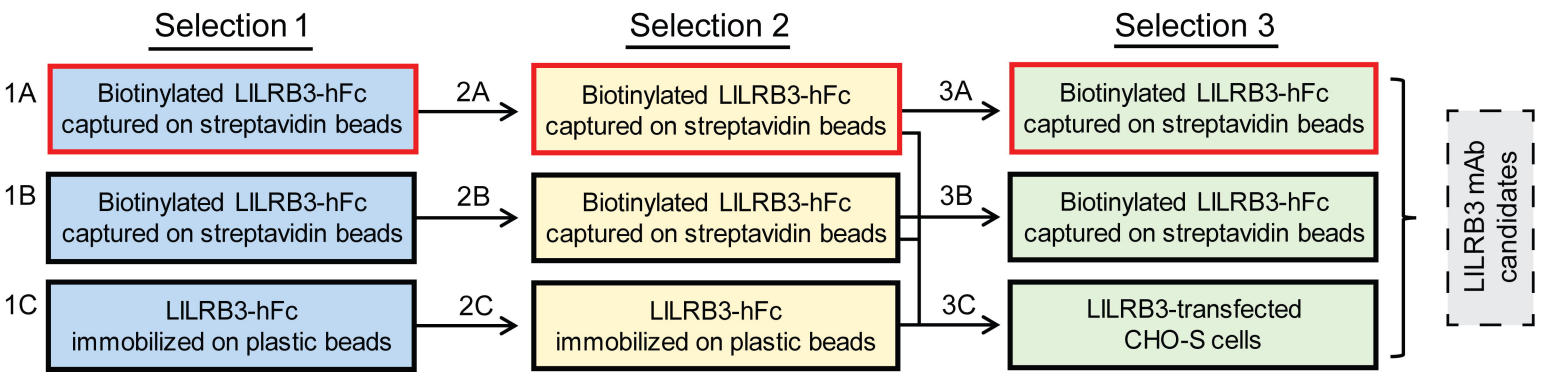
Selection 1
Selection 2
Selection 3
1A
Biotinylated LILRB3-hFc captured on streptavidin beads
2A
Biotinylated LILRB3-hFc captured on streptavidin beads
3A
Biotinylated LILRB3-hFc captured on streptavidin beads
1B
Biotinylated LILRB3-hFc captured on streptavidin beads
2B
Biotinylated LILRB3-hFc captured on streptavidin beads
3B
Biotinylated LILRB3-hFc captured on streptavidin beads
1C
LILRB3-hFc immobilized on plastic beads
2C
LILRB3-hFc immobilized on plastic beads
3C
LILRB3-transfected CHO-S cells
LILRB3 mAb candidates

Fig. S2.

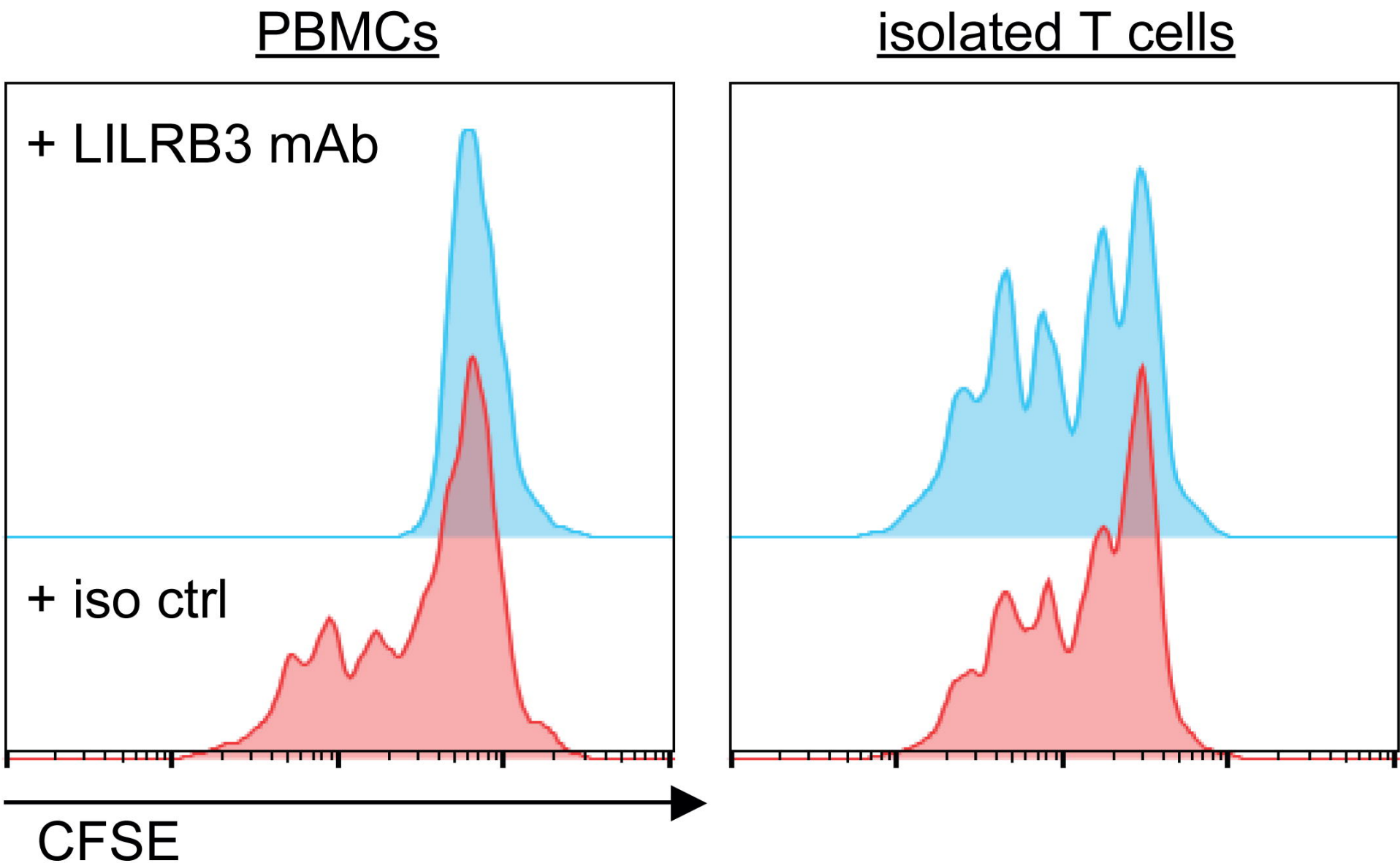
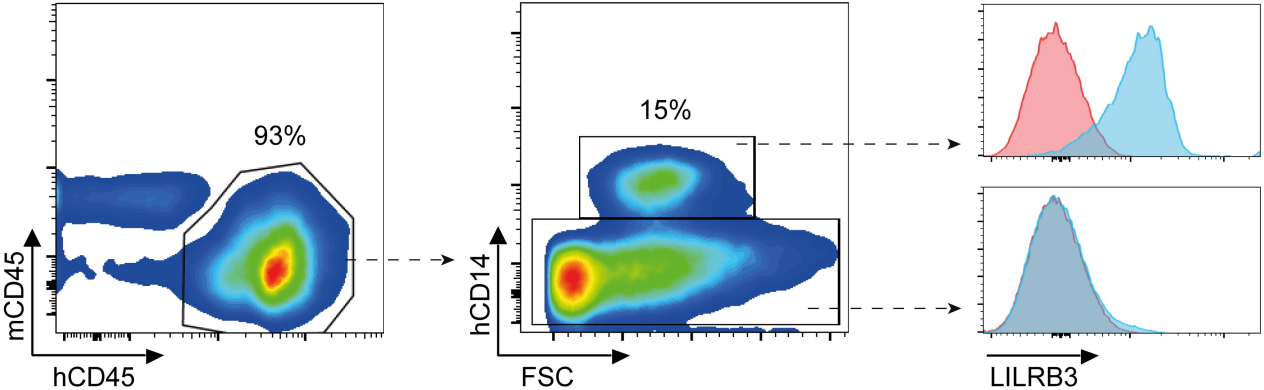
Fig. S3.